ABSTRACT

Seismic Vp & Vs Tomography of Texas and Oklahoma
with a Focus on the Gulf Coast Margin

Dominic A.D. Evanzia, M.S.

Chairman: Robert Jay Pulliam, Ph.D.

We present new 3D seismic tomography velocity models with data from 326 stations, located in Texas, Oklahoma and New Mexico, which utilized 537 seismic events. Tomography results on the North American (NA) craton show a fast anomaly outlining the southern extent. Around the Southern Oklahoma Aulacogen there is a slow anomaly, which indicates there is abundant heat present. In the Gulf Coast Plains, the NA craton shallows, allowing the ascendance of the asthenosphere. Below the craton the velocity models so a slow anomaly associated with the LAB shear zone. The slow velocity along the coast is attributed to the sediment packages. There is also a high velocity body in central/southeast Texas that has begun to delaminate from the upper crust in the region. The upper mantle structures of the Gulf Coast region suggest that the opening of the Gulf of Mexico was due to a volcanically active rifting event.

Seismic Vp & Vs Tomography of Texas and Oklahoma
with a Focus on the Gulf Coast Margin

By

Dominic A.D. Evanzia, B.S.

A Thesis

Approved by the Department of Geology

_____
Steven G. Driese, Ph.D., Chairperson

Submitted to the Graduate Faculty of
Baylor University in Partial Fulfillment of the
Requirements for the Degree
of
Master of Science

Approved by the Thesis Committee

_____
Robert Jay Pulliam, Ph.D., Chairperson

_____
John A. Dunbar, Ph.D.

_____
Gregory A. Benesh, Ph.D.

Accepted by the Graduate School
August 2013

_____
J. Larry Lyon, Ph.D., Dean

Page bearing signatures is kept on file in the Graduate School.

TABLE OF CONTENTS

LIST OF FIGURES

ACKNOWLEDGMENTS

I would like to thank my family for all of there love and support throughout my entire college career, I would not have made it this far with out their guidance and encouragement. I would also like to thank my advisor Dr. Jay Pulliam; he was of great help throughout my graduate studies at Baylor University. I would like to also thank the rest of my committee, Dr. John Dunbar and Dr. Greg Benesh, for the time and effort they put into my research project. I would also like to thank all of my fellow Baylor graduate students who provided encouragement and who were always willing to help me with my project. Finally I would like to thank my professors at Northern Arizona University, especially David Brumbaugh, who peaked my interest in seismology and geophysics and always encouraged me to continue my studies.

CHAPTER ONE

Introduction

The provocation for this research was to develop 3D velocity structure of the upper mantle structures beneath Texas and Oklahoma, recognize the association between seismic anomalies and geologic features in the region and ascertain the process which led to the opening of the Gulf of Mexico. This would not have been possible without the start of the EarthScope Transportable Array initiative, which was in place in Texas and Oklahoma from 2009 to 2012. Up to this point there was little known about the upper mantle structures in the region due to the lack of seismic instrumentation and study interest. This tomography study, in conjunction with a SKS splitting and receiver function survey also happening at Baylor University will also serve as further exploration and explanation of the Earths structures at depth beneath Texas and Oklahoma. Further more, this study will allow for the advancement of scientific knowledge of the region. I am the primary author on the submitted paper. Other authors include Ryan Ainsworth, Kevin Pratt, Jay Pulliam and Harold Gurrola. These other authors contributed by aiding in the collection, analysis, and interpretation of the data. The manuscript was submitted in an EPSL (Earth and Planetary Science Letters) format.

CHAPTER TWO

Manuscript One

Seismic Vp & Vs Tomography of Texas & Oklahoma
with a Focus on the Gulf Coast Margin

Abstract

The northwestern Gulf of Mexico passive margin contains an extensive record of continental collision and rifting, as well as deformation associated with orogenic events and heavy sedimentation. Seismic traveltime tomography that incorporates new data from 328 broadband seismic stations deployed throughout the region reveals several prominent features that correlate well with expected mantle structures, as well as features that have no obvious expression at the surface. Among the former are a large fast anomaly that corresponds to the southern extent of the Laurentia craton and a large slow anomaly associated with the Southern Oklahoma Aulacogen. Among the latter are a slow layer that we interpret to be a shear zone at the base of the cratonic and transitional continental lithosphere, a zone that is bounded at its top and bottom by discontinuities and high levels of seismic anisotropy identified in companion receiver function and shear wave splitting studies, respectively. A high velocity body underlying the Gulf Coast Plains may mark delaminating lower crust. If this is true it could provide indirect evidence that active rifting best describes the process that created the Gulf of Mexico.

1. Introduction

1.1 Geological background

The region that now comprises the northern Gulf of Mexico (GoM) and Texas's continental margin underwent several complete cycles of continental rifting and suturing before the opening of the modern GoM (Harry and Londono, 2004). These pre-GoM events included the southwest-northeast trending Grenville orogeny, which deformed Laurentia's southern margin during the late Precambrian and the Ouachita orogeny, which led to the formation of Pangea ~300 Ma (Stern et al., 2010). Rifting in the region began approximately 160-140 Ma, ultimately separating what is now Texas from the Yucatan peninsula and creating of the Gulf of Mexico (Bird et al., 2005). Several major geologic features were created after the final rift episode, including the Southern Oklahoma Aulacogen (SOA), the Rio Grande Rift (RGR), the Llano Uplift (LU), the Balcones Fault Zone (BFZ) and the Gulf Coastal Plain (GCP) (Figure 1).

The SOA is thought to be a failed rift, likely an arm of a triple junction that formed during continental break up in the Precambrian/early Paleozoic (Brewer, 1982). The current structure of the SOA is the result of deformation during the Ouachita orogeny (Baldbridge et al., 1995). The RGR trends northward from Mexico through New Mexico and into Colorado. It consists of two distinct provinces: the north, which comprises a single rift valley between the Colorado Plateau and the Great Plains, and the south, where greater extension occurred and is physiogeographically identical to the Basin and Range (Keller and Baldridge, 1999).

The Llano Uplift (LU) exposes the deformed core of the Grenville orogenic belt (Mosher, 1998) in central Texas, marking the terminus of the Edwards Plateau. The LU

is comprised of metavolcanic, metaplutonic, and metasedimentary rocks, aged 1303 – 1232 Ma (Walker, 1992). The Balcones Fault Zone (BFZ) is an extensional feature, consisting of normal faults that are located between the Edwards Plateau/Llano Uplift and the GCP (Weeks, 1945). The GCP is a passive margin that resulted from the rifting that opened the GoM. The creation of the GoM has been attributed to active volcanic rifting (Mickus et al., 2009) as well as to passive rifting (lithospheric extension) (Marton and Buffler, 1993); its true origin is therefore uncertain. The style of rifting is poorly constrained, in part, because the crust is overlain by ~15 km of sediments (Mickus et al., 2009) that were deposited between the Late Cretaceous and the Quaternary (Harry and Londono, 2004; Galloway et al., 2001; Galloway, 2008).

1.2 Previous geophysical studies

Few seismic tomography studies have been performed in the Texas/Oklahoma region, due primarily to the small number of seismic stations that have been located in the region historically. Two seismic tomography studies have been conducted recently that focus on different properties of the Rio Grande Rift, which borders the western edge of our study area. These previous studies include the La Ristra (Colorado Plateau/Rio Grande Rift Seismic Transect Experiment) deployment, which traversed the rift from the Colorado Plateau in southeast Utah to the Great Plains in west Texas (Gao et al., 2004), and the SIEDCAR (Seismic Investigation of Edge-Driven Convection Associated with the Rio Grande Rift) which focused on possible lithospheric erosion beneath western Texas and eastern New Mexico (Rockett et al., 2013). A potential field study of subsurface structure in the same region of the Texas/Gulf of Mexico transition zone

found the gravity and magnetic data to be consistent with a deeply buried volcanic rifted margin (Mickus et al., 2009).

Traveltime tomography exploits information contained within a seismic record in order to constrain 2D or 3D seismic velocity models of the Earth's subsurface (Rawlinson et al., 2010). Seismic velocity perturbations can result from variations in temperature, partial melt, and seismic anisotropy, as well as variations in chemical composition (Schmandt and Humphreys, 2010). Seismic tomography has been widely used to image upper mantle structures (e.g., Rawlinson et al., 2006; Rawlinson and Kennett, 2008; Schmandt and Humphreys, 2010), upper mantle convection (Ping et al., 2006; Schmandt and Humphreys, 2010), hotspots (Benoit et al., 2006; Schmandt et al., 2012), as well as subducting lithosphere at depth (Cheng et al., 2012). Seismic traveltime tomography, in general, involves the solution of a large inverse matrix problem in order to obtain a heterogeneous model that is most consistent with observations (Rawlinson et al., 2010). As has been shown by numerous previous studies, seismic tomography has the capacity to reveal a wide range of mantle structures and should therefore serve as a useful tool for imaging the subsurface beneath the Texas Gulf Coast passive margin.

2. Data

We use earthquakes that occurred between July 2008 and March 2013 and were recorded by twenty or more of 328 broadband, three-component stations in Texas, Oklahoma and New Mexico. Earthquakes were required to have magnitudes ranging from 5.0 to 7.0 and located at distances of 30°-95° from recording stations. Of the 328 stations, 234 were from the Earthscope Transportable Array (TA), located throughout Texas, Oklahoma, and New Mexico (see http://www.earthscope.org); 71 stations were

part of the SIEDCAR deployment (Pulliam et al., 2009), and 23 stations were from the GCP deployment that transverses the Gulf Coastal Plain (Figure 2). All stations consisted of a broadband, three-component seismometer and a 24-bit digitizer/recorder. Precise information about each station's configuration is available from the IRIS Data Management Center's website (http://www.iris.edu/dms/dmc).

The GCP broadband stations were distributed from Matagorda Island, a barrier island in the Gulf of Mexico, to Johnson City, TX, at 15-20 km spacing. The location of the transect was chosen because it is the shortest distance from the Gulf Coast shoreline to the Laurentia craton, so any remnants of suturing, deformation, and break-up might be imaged with a minimum number of stations. The GCP stations were installed in July 2010 and demobilized in March 2013; the transect was intended to provide a high-resolution 2D tomographic image of mantle structure across the transitional crust of the GCP that would, in turn, allow inferences concerning the tectonic history of Laurentia's southern margin. EarthScope's TA stations have a nominal spacing of 70 km, so images obtained from the 3D tomographic inversion aside from the GCP transect will have lower resolution.

P arrivals were measured from 406 events, producing a total of 50,102 source-receiver pairs. S arrivals were analyzed from 131 events, for a total of 14,187 source-receiver pairs (Figure 3). The difference in numbers between P- and S-wave data sets is largely due to differences in noise characteristics between P and S arrivals, which is partly due to the large sediment package beneath the study region and partly due to the fact that reverberating P energy creates higher noise levels for the later-arriving S waves.

Data were retrieved from the GCP stations approximately every three months. The data were then preprocessed using *Antelope*™ and *PASSCAL* seismic software and subsequently submitted to the Data Management Center operated by the Incorporated Research Institutions for Seismology (IRIS DMC) for archival. Data recorded by EarthScope TA stations were downloaded from the IRIS DMC. First arriving P- and S-waves were manually picked on the preprocessed data, which were recovered from the GCP deployment, as well as on the data downloaded from the IRIS DMC. The program *xcorrelate* (Brandon Schmandt, personal communication, 2009), was used to find relative delay times of first arriving P- and S-waves across the array of stations via cross-correlation (Figure 4a, b). Data incorporated into this study from the SIEDCAR deployment were retrieved from the database at the Baylor University Geophysics Laboratory. Delay times produced from the GCP, Earthscope TA, and SIEDCAR waveform data were then used as inputs for 3D tomography.

3. Tomographic inversions

FMTOMO, a Fortran software package, performs 3D traveltime tomography, using the fast marching method (FMM) (de Kool et al., 2006) in order to develop the forward step traveltime predictions, and a subspace inversion process to adjust model parameters to satisfy observed seismic data (Rawlinson and Sambridge, 2004a). FMTOMO employs an iterative non-linear scheme in which each inversion assumes local linearity and repeated iterations of FMM and subspace inversion allow velocities and traveltime perturbations to be reconciled in a manner that depends only weakly on the starting velocity model. In principle, FMTOMO should produce more accurate details of anomalies, including bounds and velocity contrasts, than inversion schemes

that perform just a single-step, linearized inversion. Other methods for iterated non-linear inversions, 3D raytracing for example, lack the computational stability and efficiency that FMM affords (Rockett et al., 2013).

3.1 Resolution Test

A synthetic resolution test is used to identify portions of a model that are likely to be well or poorly constrained for a given data set (Rawlinson et al., 2010, Rawlinson and Kennett, 2008). In this study we perform a checkerboard resolution test (Rawlinson and Kennett, 2008; Rawlinson and Fishwick, 2012; Rawlinson et al., 2006; Schmandt and Humphreys, 2010; Schmandt et al., 2012; Rockett et al., 2013). A checkerboard resolution test starts with a synthetic model consisting of alternating fast and slow velocity perturbations in the three-dimensional model space and the same source-receiver pairs found in the observed data set. Travel times for each source-receiver pair are computed through the checkerboard velocity model and then inverted using FMTOMO. Ideally the input checkerboard model would be retrieved exactly but variations in ray coverage (i.e., model sampling) and an imperfect experimental geometry (e.g., all stations are located at the Earth's surface and all waves are nearly vertically-propagating for teleseismic events) lead to smearing and trade-offs. Such effects indicate poor resolution; results of synthetic checkerboard tests therefore identify regions in the models for which resolution is relatively poor or relatively strong.

Three synthetic resolution tests were performed for both P- and S-wave tomography models. In order to investigate small- to large-scale resolution, checkerboard sizes were set to 50 km, 75 km, and 100 km (Figure 5a, b, c), respectively. Input amplitudes were set to ±0.4 km/s in each case. The checkerboard resolution tests for both

P (Figure 6a, b, c) and S (Figure 7a, b, c) models show good lateral resolution in the northwest-southeast direction to a depth of 440 km. The resolution of both the Vp and Vs models decreases from the center of the model to its boundaries, a pattern that mirrors the distribution of crossing rays in our data set. Consistent with a previous studies in the area by Rockett et al. (2013), the checkerboard tests show smearing in the northeast-southwest direction; this smearing is due to a smaller number of earthquake sources located to the southwest and northeast of the stations compared to the northwest and southeast.

The results of all of the synthetic tests display various levels of vertical smearing. Vertical smearing results from the fact that rays from teleseismic events are sub-parallel and nearly vertically-propagating when they arrive at stations, so this effect is unavoidable with the data we have available. Including local earthquakes might increase the constraints and reduce vertical smearing but the region imaged here is relatively inactive seismically, so few local events are available for inclusion. It is important to note that the vertical smearing effect makes it difficult to describe accurately the depth limits and vertical extent of anomalies.

3.2 Model Parameters

Vp and Vs models are parameterized identically; the model space is divided into two layers, with one layer above the Moho and one layer below. The two layers are represented by 7776 and 62208 velocity nodes, respectively. Nodes are spaced 25 km apart in latitude, longitude, and depth. The reference, or "initial", velocity model used for all inversions during this study is the 1D ak135 model (Kennett et al., 1995). Multiple parameterizations, consisting of various node spacing, numbers of layers, and associated

layer velocities were tested in order to explore the robustness of the inversion. All parameterizations produced similar patterns of anomalies, although the amplitudes of those anomalies varied slightly. Inversions for both the Vp and Vs models used six iterations of a 20- to 25-dimensional subspace inversion with a smoothing value of 350 and a damping value of 1. The final P-wave model solution reduces data variance from 3.922 s^2 to 1.331 s^2, a reduction of 66%. The final S-wave model solution reduces data variance from 4.055 s^2 to 1.666 s^2, a reduction of 59%. Our choices of smoothing and damping factors were based on numerous trials of a wide variety of smoothing and damping values. The final smoothing and damping factors were selected because they did not produce features that were smaller than checkerboard tests revealed to be resolvable while simultaneously resulting in a high data variance reduction. We emphasize, however, that other choices of smoothing coefficients and, to a lesser extent, damping coefficients, within a broad range did not change the pattern of anomalies sufficiently to require alternative interpretations of features from those provided below.

4. Results

Horizontal and vertical cross-sections through the final Vp and Vs 3D tomographic models display several notable features. A region of high Vp parallels the coast (Figure 8A, 8B, region b), although this anomaly is not as pronounced in the Vs model (Figure 8C, 8D). The high Vp anomaly, trends northeast/southwest across Texas from south of the Big Bend region to the border of Texas with Louisiana, while extending 450 km inland from the Texas coastline, at its maximum. The fast anomaly may continue into Mexico and Louisiana but, due to a lack of data from outside of the United States, the extent of the anomaly beyond the U.S.-Mexico border is uncertain. An

inversion that includes data from TA stations east of Oklahoma and Texas could determine whether the anomaly extends into Louisiana and beyond.

A fairly continuous slow anomaly underlies the fast anomaly throughout central Texas (Figure 9B-I, region d) but the depth to the anomaly differs between the Vp and Vs models. In the Vp model the onset of the anomaly ranges from 210 km to 270 km, the anomaly is then continuous to at least a depth of 440 km. The slow anomaly trends northeast-southwest along the coastline and deepens to the northwest. It is overlain by a region of high Vp, with few exceptions, and the fast anomaly dips around the southern edge of the slow anomaly in several locations. In the Vs model (Figure 9G) the slow anomaly starts approximately 150 km inland from the coast at a depth of 80 km, dipping northwest (as in the Vp model) and extending ~625 km inland and to a depth of ~240 km. In the Vs model, the slow anomaly is semi-continuous from its onset at 80 km (Figure 9F-I) to the bottom of the model at 440 km. The Vs GCP cross-section shows the slow anomaly with an average thickness of ~150 km, with a fragment to 440 km (Figure 9G, region d). A large slow anomaly at the surface that trends with the Texas coastline and deepens out into the Gulf of Mexico is present only in the Vs model (Figure 9F-I, region d).

A slow anomaly beneath the Texas Panhandle and western Oklahoma appears in, and correlates strongly between, Vp and Vs models (Figure 8A-D; Figure 9B-I, region a). The slow anomaly is present at the surface and continues to a depth of at least 440 km. The anomaly is more extensive near to the surface in the Vp than the Vs model.

5. Discussion

5.1 Upper Mantle Shear Zone

A large slow anomaly in the Vs tomographic model denotes a significant change in seismic velocity across the Gulf Coastal Plain and, at greater depths, beneath the cratonic lithosphere (Figure 9F-I, region d). The top of the slow velocity may mark the top of the underlying asthenosphere; this boundary corresponds to a discontinuity identified by Sp receiver function imaging in a companion study (Ainsworth et al., 2013), which those authors interpreted to be the top of a shear zone or, perhaps, the lithosphere-asthenosphere boundary (LAB). The LAB is a region of weakness where the rigid lithosphere is underlain by the weak, plastically-deforming asthenosphere (Eaton et al., 2009), and is often associated with a shear zone. Studies of SKS splitting (Comiskey et al., 2013; Refayee et al., 2013) have identified high levels of anisotropy beneath the Gulf Coastal Plain at depths of ~180 km, which would correspond to the top of the slow anomaly. A shear zone might produce slow shear wave velocities and large SKS splitting lag times as a result of partial melt, which would provide greater mobility to the asthenosphere as it flows around the cratonic keel. Note, again, that vertical limits of anomalies are not well-constrained in this (or any) tomography that relies solely on teleseismic earthquakes but the slow feature described here is quite robust with respect to perturbations of parameterizations, including node spacing, number of layers, and details of the layer boundaries.

A portion of region d (Figure 9F-I) follows the coastline and extends from the surface to a depth of ~190 km and is notably thicker than the inland portion of the anomaly. The extensive velocity anomaly can be attributed to vertical smearing between several smaller anomalies. In the crust the slow velocity results from the presence of ~15 km sediment package along the GCP and at subcrustal depths it may be due to mantle

that has been depleted as a result of melt extraction during rifting. Mickus et al. (2009) attributed an anomaly with a high magnetic susceptibility in this region to the presence of a large mafic igneous complex. This igneous complex may have resulted from melt extraction from the mantle below. Vertical smearing makes it impossible to distinguish small velocity anomalies independently. However, various tests in which the shallowest layers of the Gulf Coastal Plain were set to very slow velocities, to mimic slow velocities in the thick pile of sediments, did not change the spatial extent of the subcrustal slow Vs anomaly, only the magnitudes of the velocities.

5.2 Laurentia Craton

A large, slightly fast anomaly, shown in horizontal depth slices of the Vp and Vs models (Figure 9B- I, region b), is present beneath Texas and eastern Oklahoma and appears in a location that is largely consistent with the southern extent of the Laurentia craton. Previous studies have made use of seismic tomography as a tool to estimate the thickness of the cratonic lithosphere in North America (Van der Lee, 2002), China (Xu and Zhao, 2009), Brazil (Rocha et al., 2011) and Africa (Begg et al., 2009). These studies found large, slightly fast seismic anomalies in locations of cratonic lithosphere bounded by lower velocity layers. Figure 9B-D shows a strong, coherent fast anomaly to depths of ~220 km from, roughly, kilometer 50 to kilometer 450, where the "craton" feature is disrupted by the slow anomaly, noted above, that corresponds to the SOA. Figure 9B-I shows the depth of the cratonic lithosphere to be ~200-220 km beneath central Texas, while Figure 9F-I displays the depth to the bottom of the lithosphere to be shallowing seaward to ~80 km beneath the GCP. These results correlate well with those of Van der Lee (2002), which estimates the thickness of the lithosphere beneath Missouri, on the

craton, to be 180-200 km and beneath Massachusetts, on the continental margin, to be ~80 km.

5.3 Lower Crust

A region of high Vp follows the trend of the Grenville orogenic front from southwest to northeast across the study region (Figure 8A and 8B; Figure 9B-E, region c). Outcrops of poly-metamorphosed mafic material, including eclogite, have been found at the LU and in Marathon, TX (Mosher, 1998; Mosher et al., 2008). Eclogite can form when gabbroic lower crust is exposed to high temperatures and pressures and is of geophysical significance because of its high density, which can render the lower crust unstable over a lower-density mantle (Hacker, 1996). The presence of uplifted and exhumed eclogite in the Llano uplift, coupled with the large high velocity anomaly seen in the tomography results, suggests region b may contain eclogite. However, the spatial extent of the Grenville complex is currently unknown, due the absence of additional outcrops and the dearth of previous studies of deep structure in this region.

The presence of eclogite is only one possible explanation for the observed high-velocity anomaly. Mosher et al. (2008) suggest that the detachment of a subducted slab is responsible for the Llano uplift. If a subducted slab were still present and adhered to the crust above, it would likely produce a high velocity signature, as observed in the tomographic images, although the continued presence of a severed slab in this location hundreds of millions of years is unlikely.

5.4 Lower Crustal Delamination

The dipping of the fast anomaly displayed on both the southeast and northwest terminus hints at the fate of the lower crust beneath the GCP (Figure 10, region c). Delamination is the process by which lithospheric material (Marotta et al., 1998) becomes gravitationally unstable –denser than the underlying mantle—and then detaches and sinks (Lustrino, 2001). The collisional event that marks the Ouachita deformation might have underthrust crustal material beneath southern Laurentia and thereby thickened the crust in a zone that roughly mirrors the fast anomaly in Figure 8A and 8B and Figure 9B-E. A thickened crust could have placed the lower crust in the pressure and temperature range of the eclogite facies (Hacker, 1996). Depending on the density of the resulting high-grade metamorphic rock, the presence of an eclogitic body in the mantle beneath a broad NE-SW swath of Texas could generate a gravitationally unstable condition, resulting in the removal, or delamination, of the lower crust. This process may have been instigated by rifting, as the stretched crust fractured and allowed removal of the lower crust to occur in chunks. In that case the process would likely have begun near the rift, beneath what is now the Gulf Coastal Plain, and have propagated toward the craton, where its advance has slowed considerably or stopped.

The process of delamination has been invoked to explain anomalies observed seismically in numerous locations, including the Colorado Plateau (Levander et al., 2011), southeast Tibet (Ren and Shen, 2008), Wyoming (Foster et al., 2008), and the Banda Sea region (Fichtner et al., 2010). Through numerical modeling, Krystopowicz and Currie (2013) demonstrate that eclogitization is likely to lead to the development of a thick root during crustal shortening associated with orogenic processes and that,

ultimately, thickening and densification of the crustal root could lead to delamination in one of several modes. The mode that is most likely to have occurred beneath the GCP is a "rollback" process, in which delamination began near the rift and proceeded northwestward, perpendicular to the rift and the current coastline.

Jull and Kelemen (2001) show that the high temperatures required for mafic-ultramafic lower crustal material to sink into the mantle can only be achieved for arcs, volcanic rifted margins, or continental extension zones that are underlain by a mantle plume or beneath an area in which a substantial section of the upper mantle has been removed. The process of lower crustal delamination, if it is indeed occurring beneath the GCP, could provide indirect evidence for the existence of a "plume" or thermal anomaly in the mantle beneath the region before rifting initiated.

Delamination of lower crust and replacement by underlying asthenosphere would result in uplift of the remaining crust (Bird, 1979). It is clear that some uplift has occurred in the region of the Llano uplift (Mosher et al., 2008), but it is less clear whether there has been widespread uplift of the GCP. The overlying sediment package would serve to counter buoyancy created by the departure of densified lower crust and buoyancy forces need not be overwhelming. Krystopowicz and Currie (2013) suggest that a mere 7% difference in density between the lower crust and underlying mantle could be sufficient to trigger the removal of the lower crust, so its replacement by mantle material would not require large changes in elevation to return the region to isostacy.

5.5 Southern Oklahoma Aulacogen

The slow velocity anomaly, region a, found in both tomography models, located beneath the Texas panhandle and western Oklahoma (Figure 8A-D; Figure 9B-I, region

a) corresponds geographically to the SOA. The slow velocity anomaly follows the trend of the SOA, northwest-southeast through northern Texas and southwestern Oklahoma. A slow anomaly is to be expected in the region of the SOA as a result of the elevated geotherm that accompanies rift systems. The SOA has been determined by gravity and magnetic surveys to be a relatively small feature at the Earth's surface, limited to a narrow band in Oklahoma with a small extension into the Texas Panhandle (Figure 1; Robbins and Keller, 1992). Results of this tomography study show the SOA's influence extends over a much larger area and depth range than has been apparent previously. The small expression of the SOA in the Vs tomography near the surface (Figure 8C-D, region a) likely highlights only the slowest regions, such as feeder dikes or areas in which fluids are present. The surface extent of the SOA in the Vs tomography model closely resembles the expression of the SOA in gravity and magnetic studies (Robbins and Keller, 1992). A similar tomography study conducted in the RGR region (Rockett et al., 2013) also shows a large slow anomaly extending to depths of at least 440 km associated with that rift system. The RGR is undergoing active spreading, whereas spreading at the SOA appears to have ceased (*Brewer*, 1982). Similarities between the SOA and the RGR, particularly with respect to the size of each anomaly and its depth extent, suggest that the processes by which each "rift" is supplied may also be similar, and that the SOA may still be "active", in some sense, in the subsurface, even though it appears to be quiescent at the surface. Estimates of seismic anisotropy from SKS splitting measurements (Gao et al., 2008; Refayee et al., 2013; Comiskey et al., in prep, 2013) suggest that the SOA may have served as a conduit for easily deformable or mobile material, due to the alignment of fast polarization vectors with the trend of the rift. If the

material is truly mobile, the SOA may represent a pathway for asthenospheric flow around the keel of Laurentia's cratonic keel, which has been disrupted and thinned by a thermal anomaly associated with the SOA.

6. Conclusions

The region now known as Texas and Oklahoma has witnessed an extensive and complex set of orogenic, extensional, and rifting events, beginning (perhaps) with the Grenville orogeny and culminating in the opening of the GoM. Remnants of these events are likely to have been recorded in structures that now reside in the upper mantle and lower crust beneath the region. In order to gain a better understanding of the tectonic history of the region, we conducted a 2.5-year broadband seismograph transect across the GCP to collect unique data at close station spacing across the Gulf Coastal Plain and combined those data with data from two additional seismic networks. We used the combined data set to construct Vp and Vs models for the crust and mantle via traveltime tomography. The resulting tomographic images display a variety of large and small anomalies that correlate well with what is known about the region's tectonic history.

For example, a large high velocity anomaly, region b, in central Texas and eastern Oklahoma, extending to a depth of ~240 km, marks the boundary and southernmost extent of the mesoproterozoic craton. The cratonic lithosphere is underlain by a low velocity anomaly, region d, that may be associated with an upper mantle shear zone whose upper bound may represent the lithosphere-asthenosphere boundary. A slow anomaly appears beneath the Laurentia craton and the anomaly becomes shallower as it traverses the GCP to the Gulf of Mexico. Most of the fast Vp anomalies are underlain by slow Vs anomalies, which may correspond to a layer of partial melt that marks the top of

a shear zone or the LAB. Our Vp and Vs models show significant differences beneath the Gulf Coast; Vp is normal to slightly fast while Vs is unusually slow. Beneath the craton, on the other hand, Vp is quite fast and Vs is slightly fast.

A large slow velocity anomaly, region a, is present beneath the SOA. Figure 9E-H shows continuity of the slow Vs anomalies at depth between the GCP and the SOA, suggesting they may be some connection and interaction between the two anomalies. The SOA anomaly suggests that this zone may still have elevated temperatures; its apparent subsurface connection to the RGR may hint at a potential for reactivation in the future.

A high velocity anomaly, region c, is found beneath central and southeast Texas that we attribute either to densification of the lower crust and/or the presence of an unusually thick crust, perhaps resulting from continental collision at the onset of the Ouachita orogeny. The presence of eclogite in the Llano uplift suggests that some eclogite may be present in the material.

An intriguing anomaly appears beneath the GoM coast at the border between Texas and Mexico (Figure 8B). Although the anomaly is mirrored in both Vp and Vs models, it occurs in a region of poor resolution, so it does not warrant serious attention or interpretation.

The interpretation of observed structure as lower crustal delamination, if correct, may provide indirect evidence for an "active" rifting process, involving a thermal anomaly in the mantle that led to the opening of the GoM.

Acknowledgements: We thank the EarthScope Program and the Incorporated Research Institutions for Seismology (IRIS) Data Management Center (DMC) for their roles in

acquiring, archiving, and disseminating broadband seismic data on an unprecedented scale in Texas and Oklahoma. We thank Nick Rawlinson for the FMTOMO software and Brandon Schmandt for the *xcorrelate* program. J.P. and H.G. thank Bob Stern, Libby Anthony, Randy Keller, and Harm Van Avendonk for discussions that stimulated the data acquisition and research presented here. Funding is gratefully acknowledged from the National Science Foundation (EAR 0746321, EAR 0750711), the Norman Hackerman Advanced Research Program (Award # 003658-0034-2009), the Gulf Coast Association of Geological Societies, and the W.M. Keck Foundation

REFERENCES

Ainsworth, R., Evanzia, D., Pulliam, J., and Gurrola, H., 2013. Sp Receiver Function Imaging of a Passive Margin: Transect Across Texas's Gulf Coastal Plain, submitted to Earth Planet. Sci. Lett., June 2013.

Baldridge, W. S., Keller, G. R., Haak, V., Wendlandt, E., Jiracek, G. R., and Olsen, K. H., 1995. Rio Grande rift, K. H. Olsen (Eds.), Continental Rifts: Evolution, Structure, and Tectonics, Developments in Geotectonics, vol. 25, pp. 233-276, Elsevier, Amsterdam.

Begg, G. C., Griffin, W. L., Natapov, L. M., O'Reilly, S. Y., Grand, S. P., O'Neill, C. J., Hronsky, J. M. A., Djomani, Y. P., Swain, C. J., Deen, T., and Bowden, P., 2009. The lithosphere architecture of Africa: Seismic tomography, mantle petrology, and tectonic evolution, Geosphere, 5(1), 23-50. doi: 10.1130/GES00179.1.

Benoit, M., Nyblade, A., and VanDecar, J., 2006. Upper mantle P-wave speed variations beneath Ethiopia and the origin of the Afar hotspot. Geology, 34, 329-332. doi: 10.1130/G22281.1.

Bird, D. E., Burke, K., Hall, S. A., and Casey, J. F., 2005. Gulf of Mexico tectonic history: Hotspot tracks, crustal boundaries, and early salt distribution, AAPG Bull., 89, 311-328.

Brewer, J. A. (1982), Study of Southern Oklahoma Aulacogen, using COCORP deep-seismic-reflection profiles, Oklahoma Geological Survey Guidebook, 21, 31-39.

Cheng, W., Hsu, S., and Chang, H., 2012. Tomography of the southern Taiwan subduction zone and possible emplacement of crustal rocks into the forearc mantle, Global Planet. Change, 90-91, 20-28. doi: 10.1016/j.gloplacha.2012.01.003.

Comiskey, C., Pulliam, J., and Gurrola, H., 2013. Seismic Anisotropy in Texas and Oklahoma and its Relationship to Tectonic Events That Shape Southern Laurentia, in prep., June 2013.

de Kool, M., Rawlinson, N., and Sambridge, M., 2006. A practical grid-based method for tracking multiple refraction and reflection phase in three-dimensional heterogeneous media, Geophys. J. Inter., 167, 253-270. doi: 10.1111/j.1365-246X.2006.03078.x.

Eaton, D. W., Darbyshire, F., Evans, R. L., Grutter, H., Jones, A. G., Yuan, X., 2009. The elusive lithosphere-asthenosphere boundary (LAB) beneath cratons, Lithos., 109, 1-22. doi: 10.1016/j.lithos.2008.05.009.

Fouch, M. J., James, D. E., Vandecar, J. C., Lee, S. V. D., and the Kaapvaal Seismic Group, 2004. Mantle seismic structure beneath the Kaapvaal and Zimbabwe Craton, S. Afr. J. Geol., 107, 33-44.

Galloway, W.E., Whiteaker, T. L., and Ganey-Curry, P. E., 2001. History of Cenozoic North American drainage basin evolution, sediment yield, and accumulation in the Gulf of Mexico, Geosphere, 7, 938-973. doi:10.1130/GES00647.1.

Galloway, W.E. (2008), Depositional evolution of the Gulf of Mexico sedimentary basin, in K.J. Hsu, ed., Sedimentary basins of the world, v. 5, The sedimentary basins of the United States and Canada, Miall, A.D., ed.: The Netherlands, Elsevier, 505-549.

Gao, W., Grand, S. T., Baldridge, W. S., Wilson, D., West, M., Ni, J. F., and Aster, R., 2004. Upper mantle convection beneath the central Rio Grande rift imaged by P and S wave tomography, J. Geophy. Res., 109, B03305. doi:10.1029/2003JB002743.

Hacker, B. R. (1996), Eclogite Formation and the Rheology, Buoyancy, Seismicity, and H20 Content of Oceanic Crust, Geophy. Monog., 96, 337-346.

Harry, D. and Londono, J., 2004. Structure and evolution of the central Gulf of Mexico continental margin and coastal plain, southeast United States, GSA Bull., 116(1/2), 188-199. doi:10.1130/B25237.1.

Huerta, A. D. and Harry, D. L., 2012. Wilson cycles, tectonic inheritance, and rifting of the North American Gulf of Mexico continental margin, Geosphere, 8, 374-385. doi: 10.1130/GES00725.1.

Keller, G. R. and Baldridge, S. W., 1999. The Rio Grande rift: A geological and geophysical overview, Rocky Mountain Geology, 34 (1), 121-130.

Kennett, B. L., Engdahl, E. R., and Buland, R., 1995. Constraints on seismic velocities in the Earth from travel times, Geophys. J. Int., 122, 108 -124.

Krystopowicz, N. J. and Currie, C., 2013. Crustal eclogitization and lithosphere delamination in orogens, Earth Planet. Sci. Lett., 361, 195-207. doi: 10.1016/j.epsl.2012.09.056.

Lustrino, M., 2001. Debated topics of modern igneous petrology, Per. Mineral., 70(1), 1-26.

Lustrino, M., 2005. How the delamination and detachment of lower crust can influence basaltic magmatism, Earth-Sci. Rev., 72, 21-38. doi: 10.1016/j.earscirev.2005.03.004.

Marotta, A. M., Frenandez, M., Sabadini, R., 1998. Mantle unrooting in collisional settings, Tectonophysics, 296, 31-46.

Marton, G. and Buffler, R. T., 1993. Application of simple-shear model to the evolution of passive continental margins of the Gulf of Mexico basin, Geology, 21, 495-498.

Mickus, K., Stern, R. J., Keller, G. R., and Anthony, E Y., 2009. Potential field evidence for a volcanic rifted margin along the Texas Gulf Coast, Geology, 37, 387-390. doi: 10.1130/G25465A.1.

Mosher, S., 1998. Tectonic evolution of the southern Laurentian Grenville orogenic belt, GSA Bull., 110(11), 1357-1375. doi: 10.1130/0016-7606.

Mosher, S., Levine, J. S. F., and Carlson, W. D., 2008. Mesoproterozoic plate tectonics: A collisional model for the Grenville-aged orogenic belt in the Llano uplift, central Texas, Geology, 36(1), 55-58. doi: 10.1130/G24049A.1.

Ping, X., Rong-shan, F., Jain-pingm, H., Xian-jie, Z., and Zhi-yang, D., 2006. Upper mantle convection beneath northwest China and its adjacent region driven by density anomaly, ACTA Seismologica Sinica, 19, 552-562.

Pulliam, J., Rockett, C. V., and Grand, S. P., 2009. Seismic anisotropy of the Rio Grande rift and surrounding regions, AGU, Fall Meet., Abstract T53D-1623.

Rawlinson, N. and Sambridge, M., 2004a. Multiple reflection and transmission phases in complex layered media using a multistage fast marching method, Geophysics, 69, 1338-1350. doi: 10.1190/1.1801950.

Rawlinson, N. and Sambridge, M., 2004b. Wavefront evolution in strongly heterogeneous layered media using the fast marching method, Geophys. J. Int., 156, 631-647.

Rawlinson, N., Kennett, B., and Heintz, M., 2006. Insights into the structure of the upper mantle beneath the Murray Basin from 3D teleseismic tomography, Aust. J. Earth Sci., 53, 595-604. doi: 10.1080/08120090600686751.

Rawlinson, N. and Kennett, B., 2008. Teleseismic tomography of the upper mantle beneath the southern Lachlan Orogen, Australia. Phys. Earth Planet. Inter., 167, 84-97.

Rawlinson, N., Pozgay, S., and Fishwick, S., 2010. Seismic tomography: A window into deep Earth, Phys. Earth Planet. Inter., 178, 101-135. doi: 10.1016/j.pepi.2009.10.002.

Rawlinson, N. and Fishwick, S., 2012. Seismic structure of the southeast Australian lithosphere from surface and body wave tomography, Tectonophysics, 572-573, 111-122. doi: 10.1016/j.tecto.2011.11.016.

Refayee, H. A., Yang, B. B., Liu, K. H., and Gao, S. S., 2013. Mantle flow and lithosphere-asthenosphere coupling beneath the southwestern edge of the North American craton: Constraints from shear-wave splitting measurements, Earth Planet. Sci., in press.

Robbins, S. L. and Keller, G. R., 1992. Complete Bouguer and isostatic residual gravity maps of the Anadarko Basin, Wichita Mountains, and surrounding areas, Oklahoma, Kansas, Texas, and Colorado, U. S. Geological Survey, Reston, VA, United States.

Rocha, M. P., Schimmel, M., and Assumpcao, M., 2011. Upper-mantle seismic structure beneath SE and Central Brazil from P- and S-wave regional traveltime tomography, Geophys. J. Int., 184, 268-286. doi: 10.1111/j.1365-246X.2010.04831.x.

Rockett, C., Pulliam, J., and Grand, S. P., 2013. Seismic Tomographic Imaging Reveals Possible Lithospheric Erosion beneath Trans-Pecos Texas and Southeastern New Mexico, in prep., June 2013.

Schmandt, B., and Humphreys, E., 2010. Seismic heterogeneity and small-scale convection in the southern California upper mantle, Geochem. Geophy. Geosyst., 11, 1-19. doi: 10.1029/2010GC003042.

Schmandt, B., Dueker, K., Humphreys, E., and Hansen, S., 2012. Hot mantle upwelling across the 660 beneath Yellowstone, Earth Planet. Sci. Lett., 331-332, 224-236. doi: 10.1016/j.epsl.2012.03.025.

Seager, W. R., Morgan, P., and Riecker, R. E., (Eds.) 1979. Rio Grande Rift in southern New Mexico, West Texas, and northern Chihuahua, in Rio Grande Rift: Tectonics and Magmatism, pp. 87-106, AGU, Washington, D. C..

Stern, R., Dickinson, W. R., Lawton, T., 2010. Introduction: Making the Southern Margin of Laurentia, Geosphere, 6(6), 737-738. doi: 10.1130/GES00642.1.

Van der Lee, S., 2002. High-resolution estimates of lithosphere thickness from Missouri to Massachusetts, USA, Earth Planet. Sci. Lett., 203, 15-23.

Walker, N. W., 1992. Middle Proterozoic geologic evolution of Llano uplift, Texas: Evidence from U-Pb zircon geochronometry. GSA Bull., 104, 494-504. doi: 10.1130/0016-7606.

Weeks, A. W., 1945. Balcones, Luling, and Mexia fault zones in Texas, AAPG Bull., 29(12), 1733-1737. doi: 10.1306/3D9337B0-16B1-11D7-8645000102C1865D.

Wilson, D., Aster, R., West, M., Ni, J., Grand, S., Gao, W., Balridge, S. W., Semken, S., and Patel, P., 2005. Lithospheric structure of the Rio Grande rift, Nature, 433, 851-855. doi: 10.1038/nature03297.

Xu, P. and Zhao, D., 2009. Upper-mantle velocity structure beneath the North China Craton: implications for lithosphere thinning, Geophy. J. Int., 177, 1279-1283. doi: 10.1111/j.1365-246X.2009.04120.x.

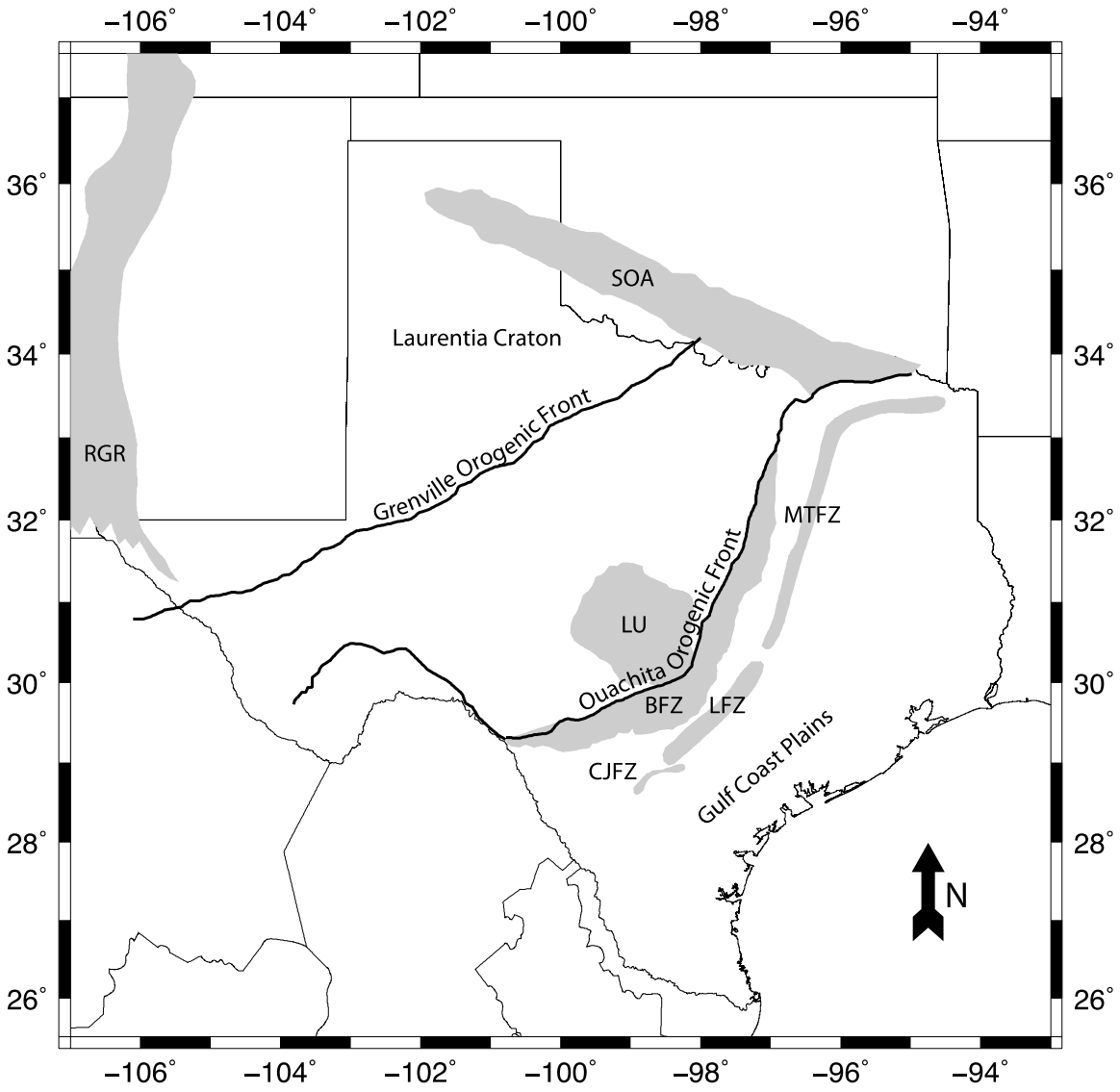

Figure 1:Tectonic map of Texas and Oklahoma: Map of Texas and Oklahoma displaying relative locations of significant tectonic features as they pertain to the Laurentia Craton and the Gulf Coast Plains. Regions of deformation and/or uplift (shaded) and include: the Rio Grande Rift (RGR), the Southern Oklahoma Aulacogen (SOA), the Llano Uplift (LU), the Balcones Fault Zone (BFZ), the Mexia-Talco Fault Zone (MTFZ), the Luling Fault Zone (LFZ) and the Charlotte-Jourdanton Fault Zone (CJFZ). Orogenic fronts (solid lines) include the Grenville orogenic front and the Ouachita orogenic front.

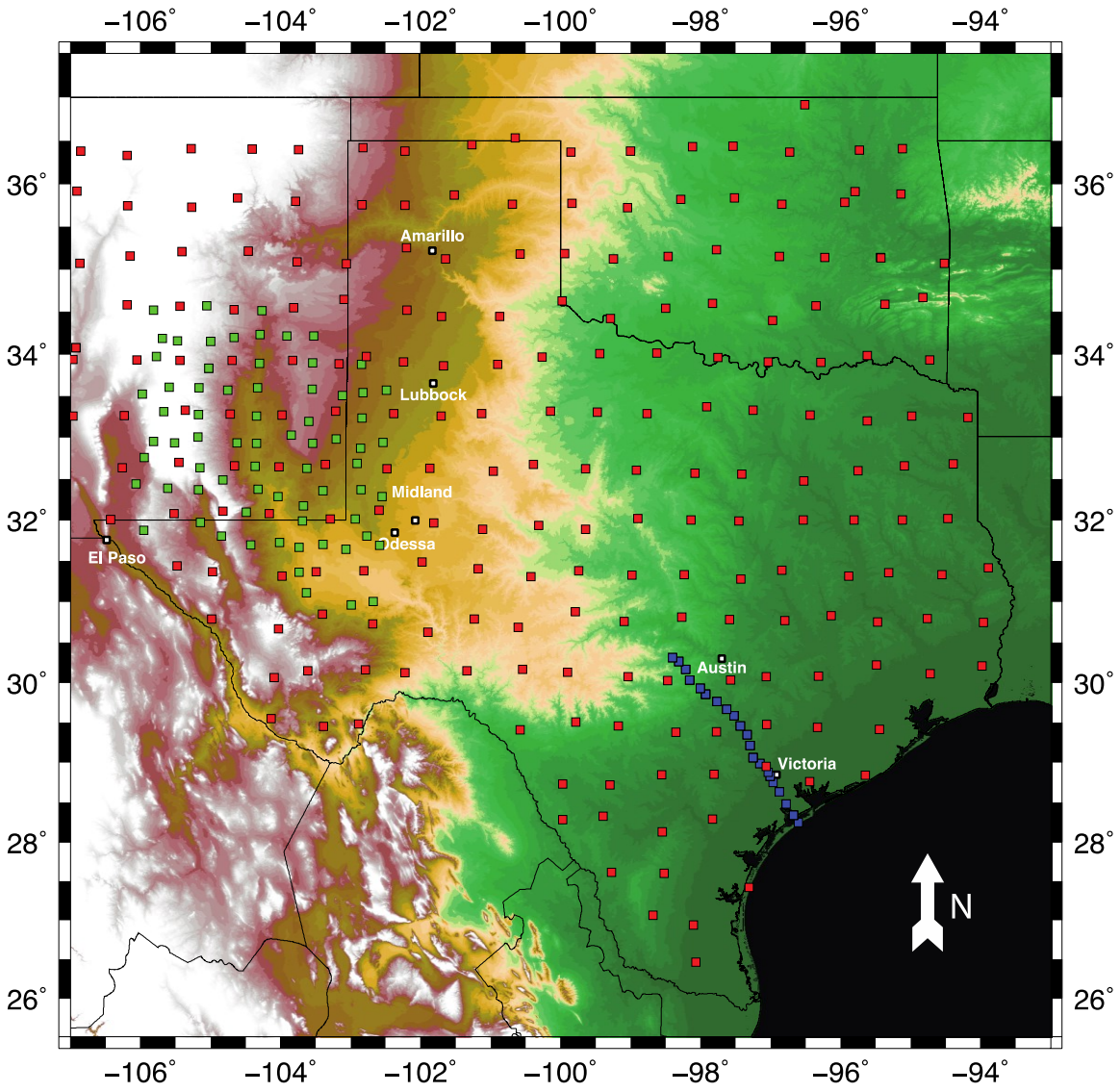

Figure 2: Station location map: The X4 Network (Blue) associated with the GUMBO project is intermixed with the XR Network (Green) associated with the SIEDCAR project and the TA (Transportable Array) Network (Red) associated with Earthscope.

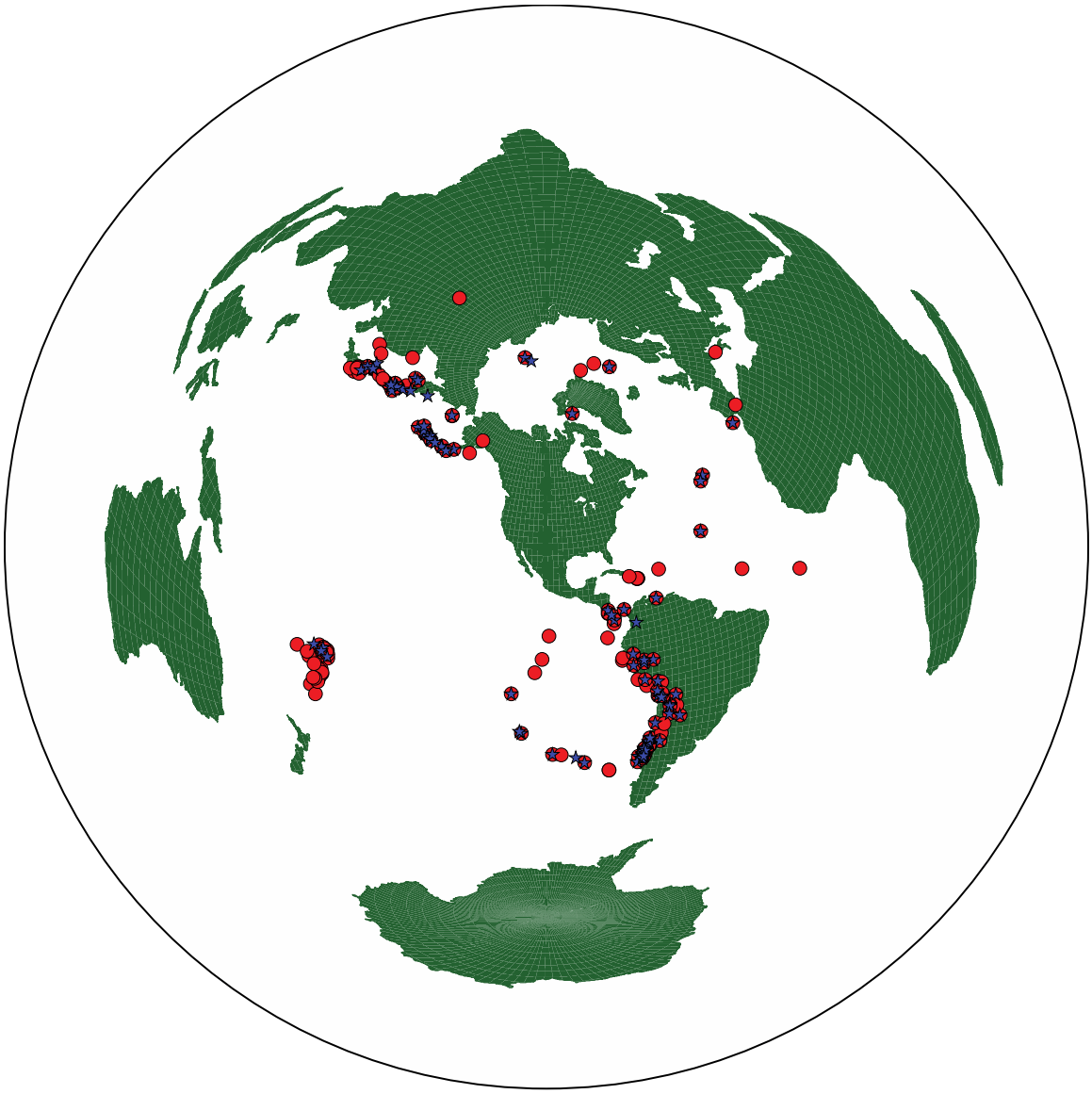

Figure 3: Earthquake location map: Azimuthal distribution of the 537 (P-wave: 406; S-wave: 131) earthquakes of magnitude ≥ 5.0 used in the compressional (red circles) and shear (blue stars) wave inversion. All teleseismic sources have distances 30-90° from the array (center of plot).

A

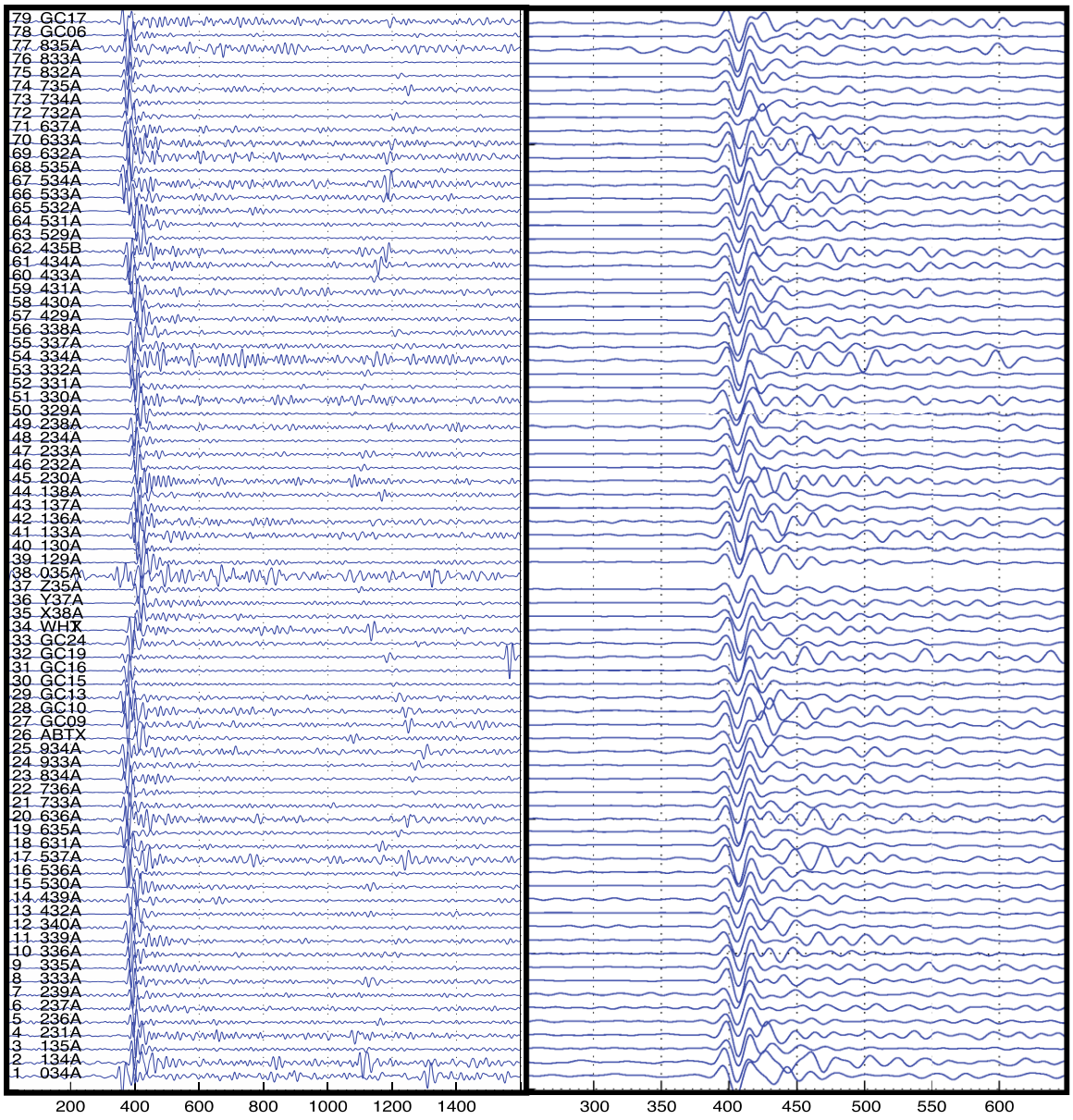
79 GC17
78 GC06
77 835A
76 833A
75 832A
74 735A
73 734A
72 732A
71 637A
70 633A
69 632A
68 535A
67 534A
66 533A
65 532A
64 531A
63 529A
62 435B
61 434A
60 433A
59 431A
58 430A
57 429A
56 338A
55 337A
54 334A
53 332A
52 331A
51 330A
50 329A
49 238A
48 234A
47 233A
46 232A
45 230A
44 138A
43 137A
42 136A
41 133A
40 130A
39 129A
38 035A
37 Z35A
36 Y37A
35 X38A
34 WHX
33 GC24
32 GC19
31 GC16
30 GC15
29 GC13
28 GC10
27 GC09
26 ABTX
25 934A
24 933A
23 834A
22 736A
21 733A
20 636A
19 635A
18 631A
17 537A
16 536A
15 530A
14 439A
13 432A
12 340A
11 339A
10 336A
9 335A
8 333A
7 239A
6 237A
5 236A
4 231A
3 135A
2 134A
1 034A
200
400
600
800
1000
1200
1400
300
350
400
450
500
550
600

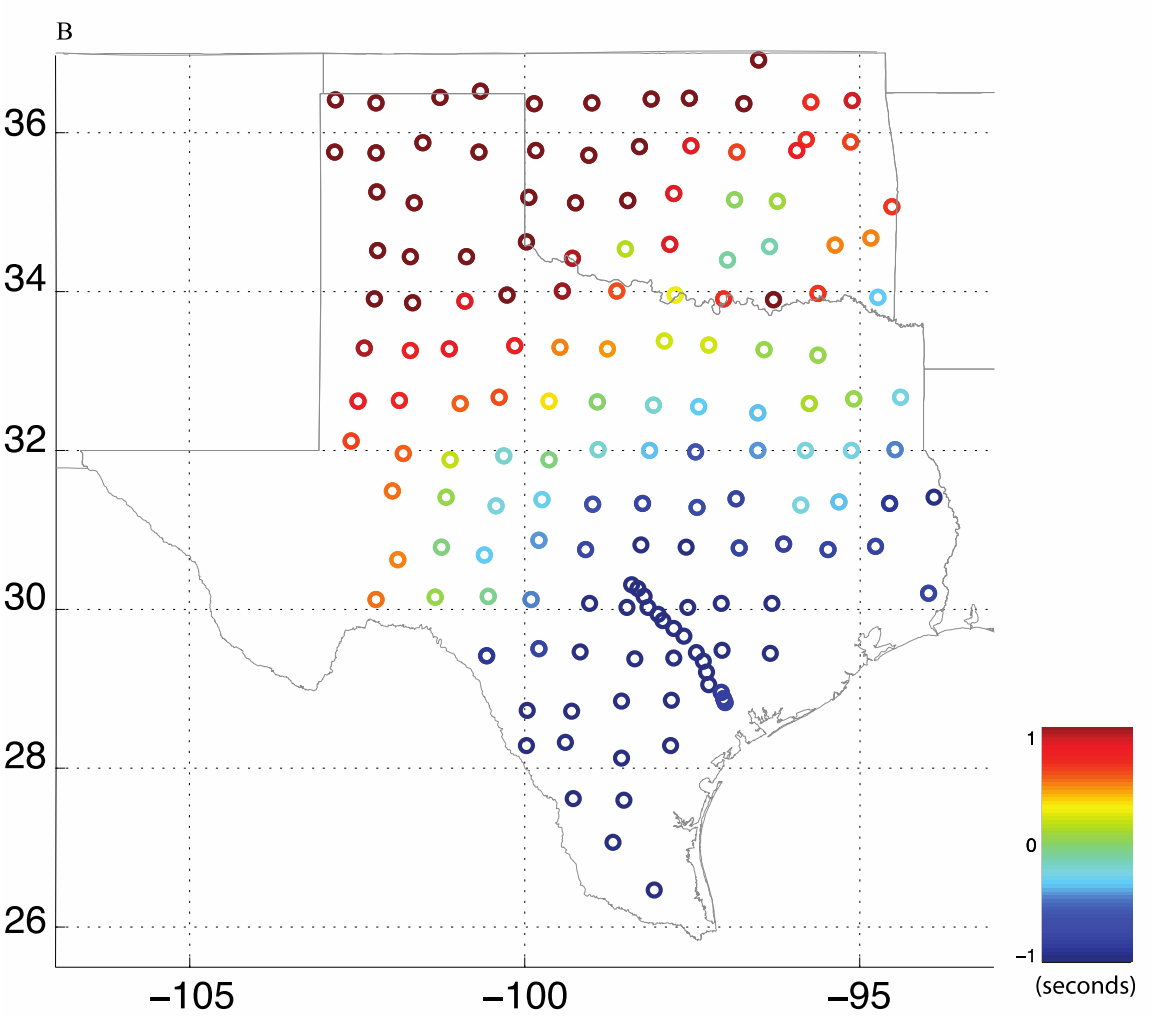

Figure 4: Xcorrelate: (A) Labeled by station (Y-axis) and node points (X-axis), Sample of initial input of waveforms for Xcorrelate (left), counterpart of previous waveforms after cross-correlation is preformed (right), (B) Calculated delay times (seconds) represented by colored circles.

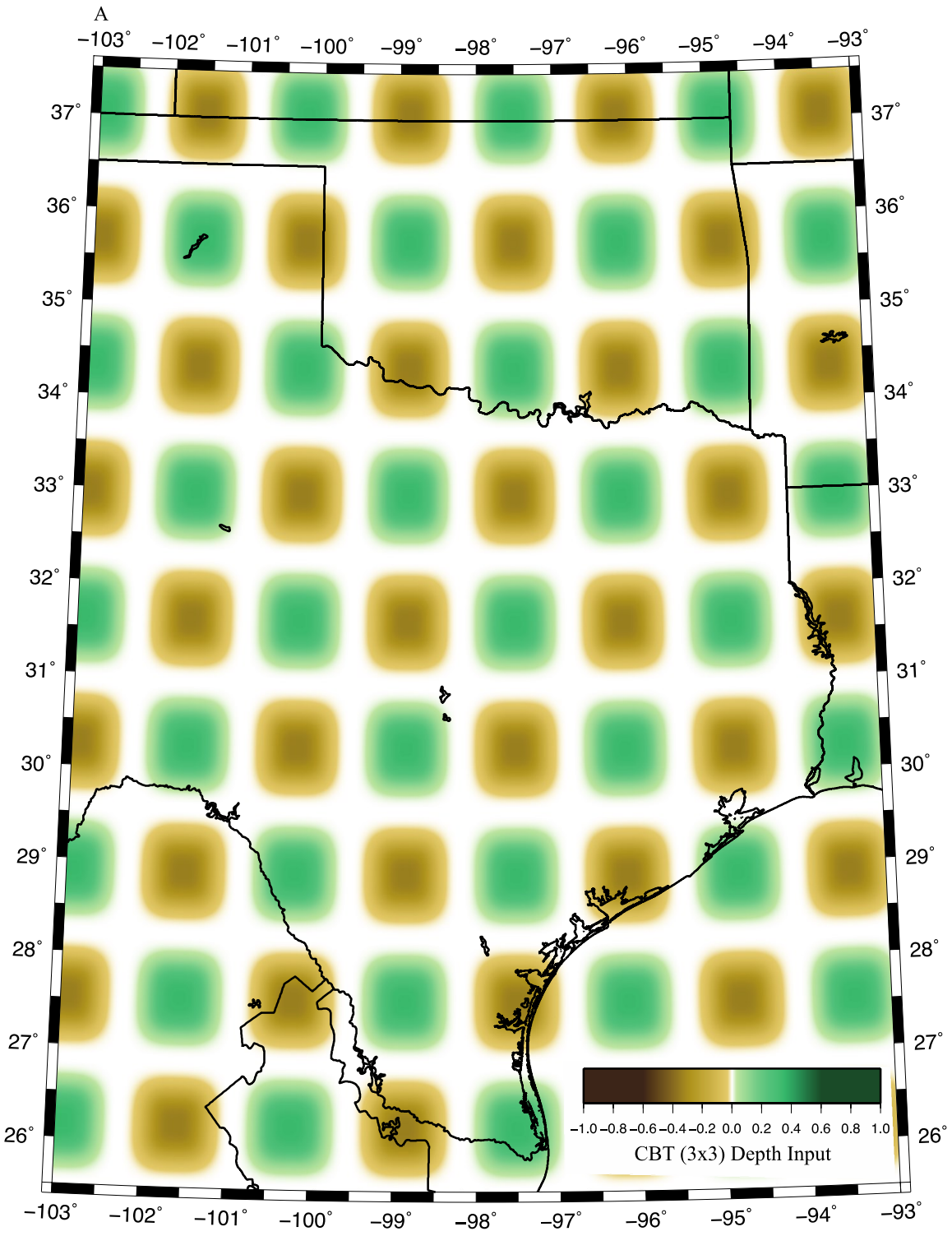
A
−103°
−102°
−101°
−100°
−99°
−98°
−97°
−96°
−95°
−94°
−93°
37°
36°
35°
34°
33°
32°
31°
30°
29°
28°
27°
26°
−1.0 −0.8 −0.6 −0.4 −0.2 0.0 0.2 0.4 0.6 0.8 1.0
CBT (3x3) Depth Input

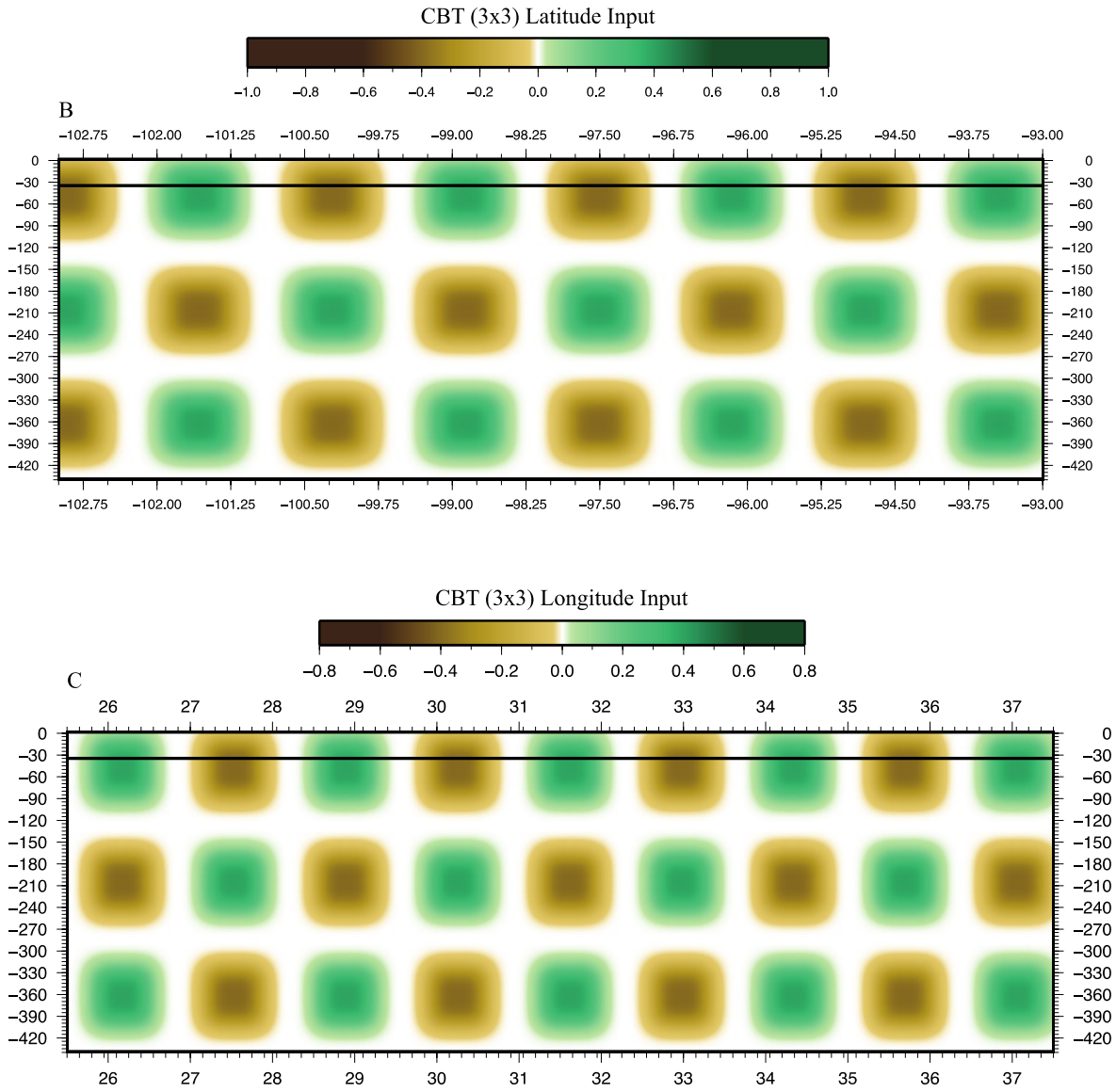

Figure 5: Reference checkerboard model: Input for resolution test of the compressional and shear model with checkerboard sizes of 3x3 velocity nodes equaling ~75 km^3 per perturbation node. (A) depth slice, (B) latitude slice and (C) longitude slice.

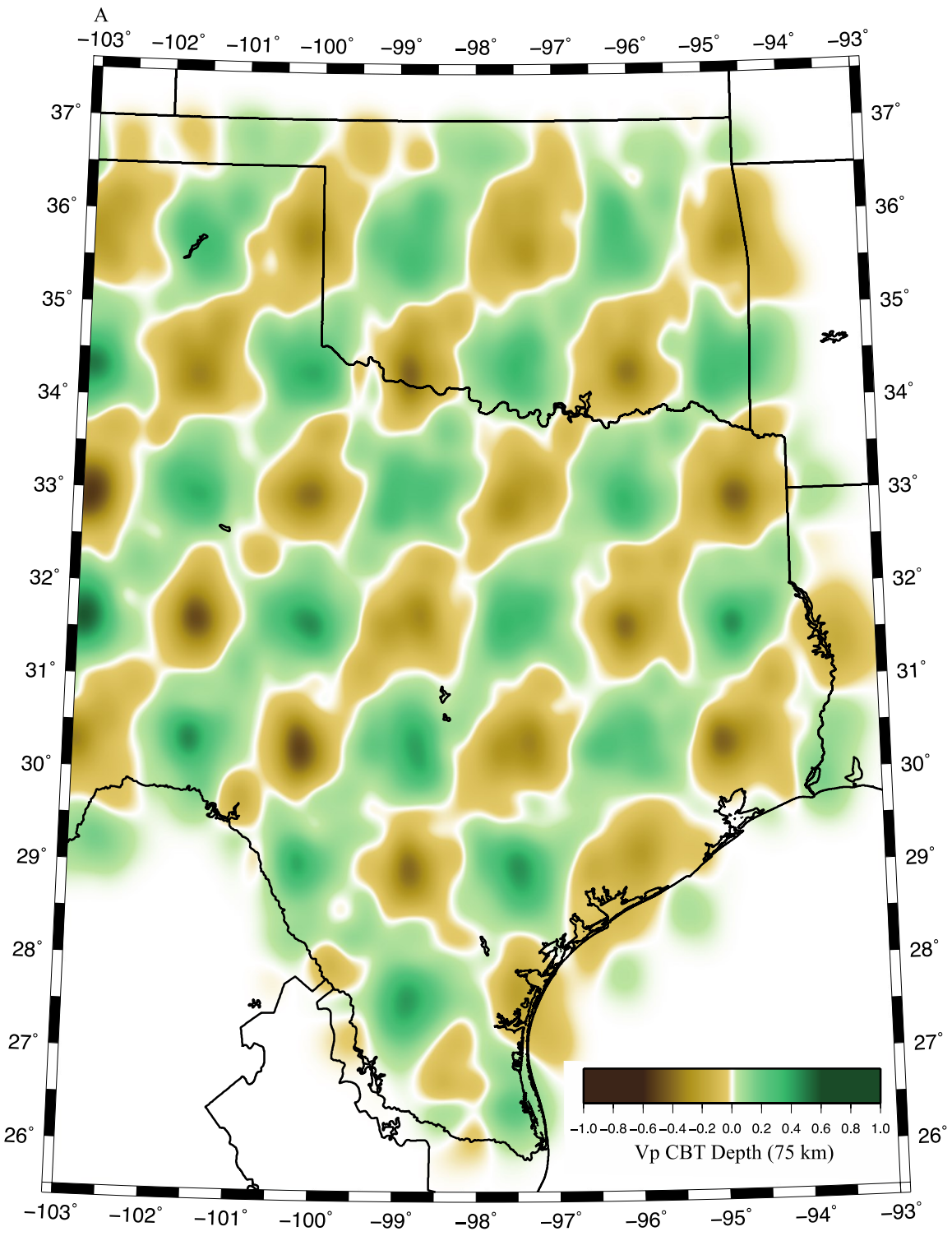
A
−103°
−102°
−101°
−100°
−99°
−98°
−97°
−96°
−95°
−94°
−93°
37°
36°
35°
34°
33°
32°
31°
30°
29°
28°
27°
26°
−1.0 −0.8 −0.6 −0.4 −0.2 0.0 0.2 0.4 0.6 0.8 1.0
Vp CBT Depth (75 km)

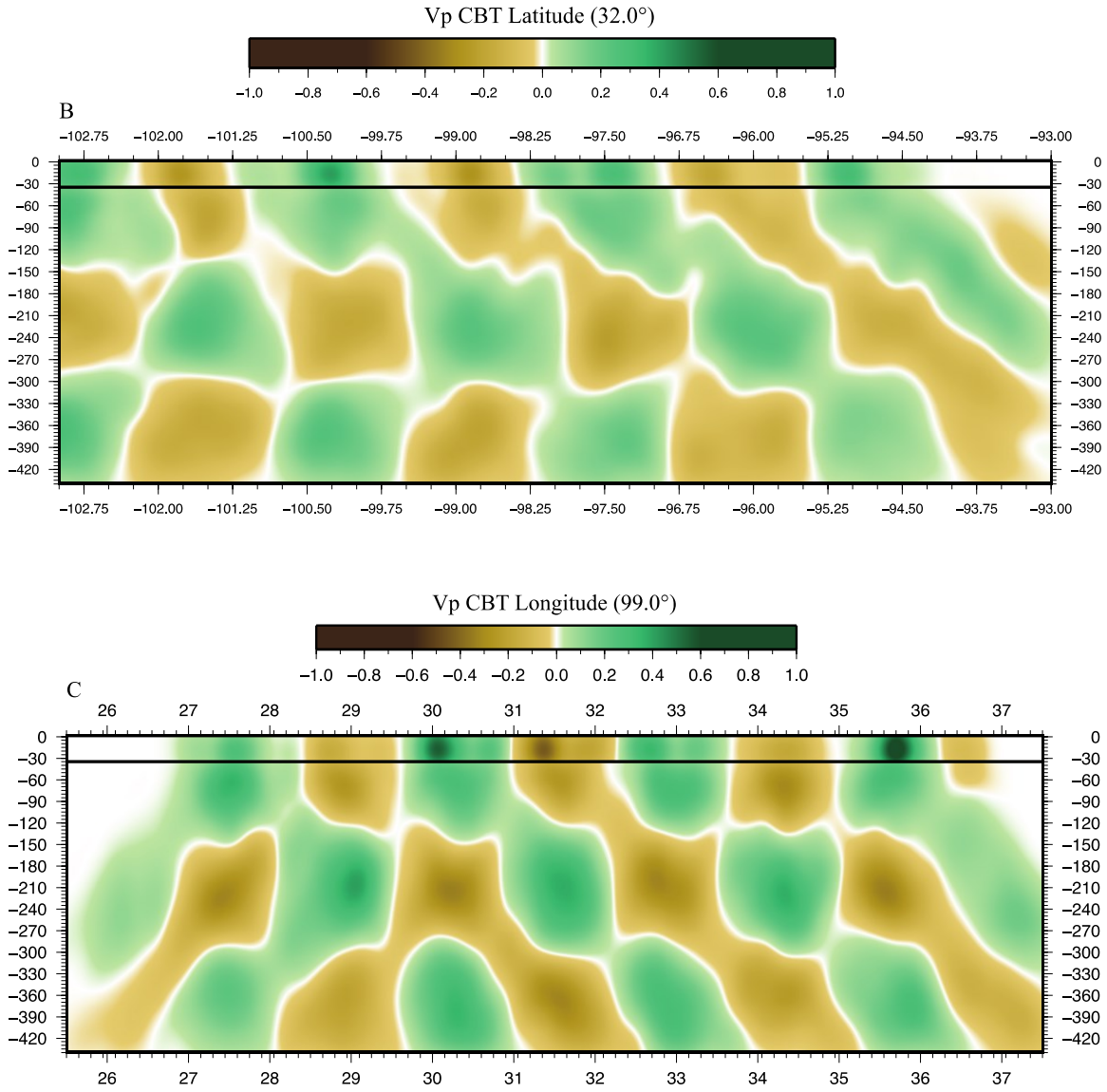

Figure 6: Vp checkerboard test result: (A) 75 km depth slice: displaying good resolution throughout the study area with little smearing to the northeast-southwest, (B) Latitude (32.0°) slice displaying overall good west to east resolution in the study area, with little smearing in the west and progressively increasing smearing to the east, (C) Longitude (99.0°) slice displaying reasonable south to north resolution with some smearing (north to south).

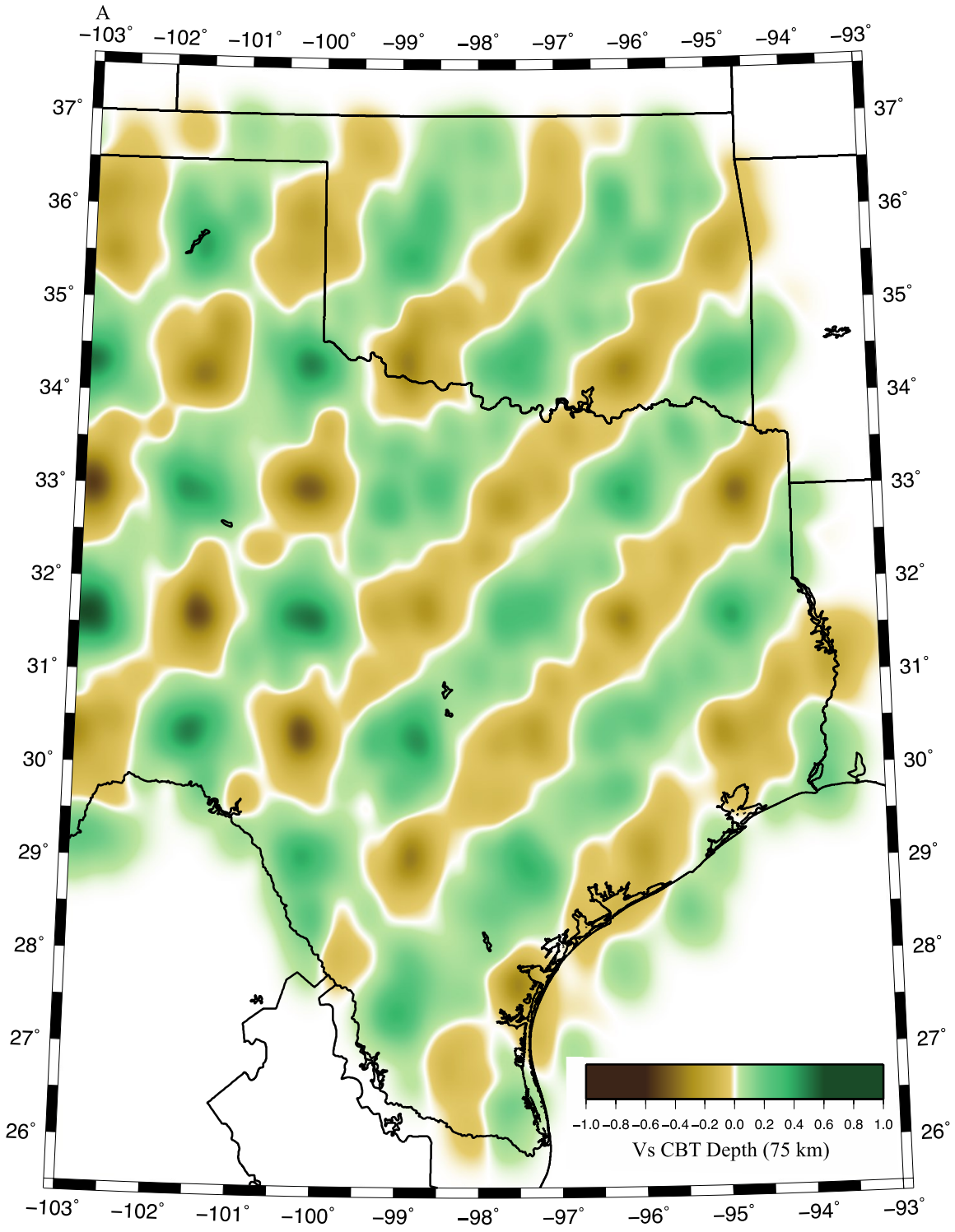
A
−103°
−102°
−101°
−100°
−99°
−98°
−97°
−96°
−95°
−94°
−93°
37°
36°
35°
34°
33°
32°
31°
30°
29°
28°
27°
26°
−1.0 −0.8 −0.6 −0.4 −0.2 0.0 0.2 0.4 0.6 0.8 1.0
Vs CBT Depth (75 km)

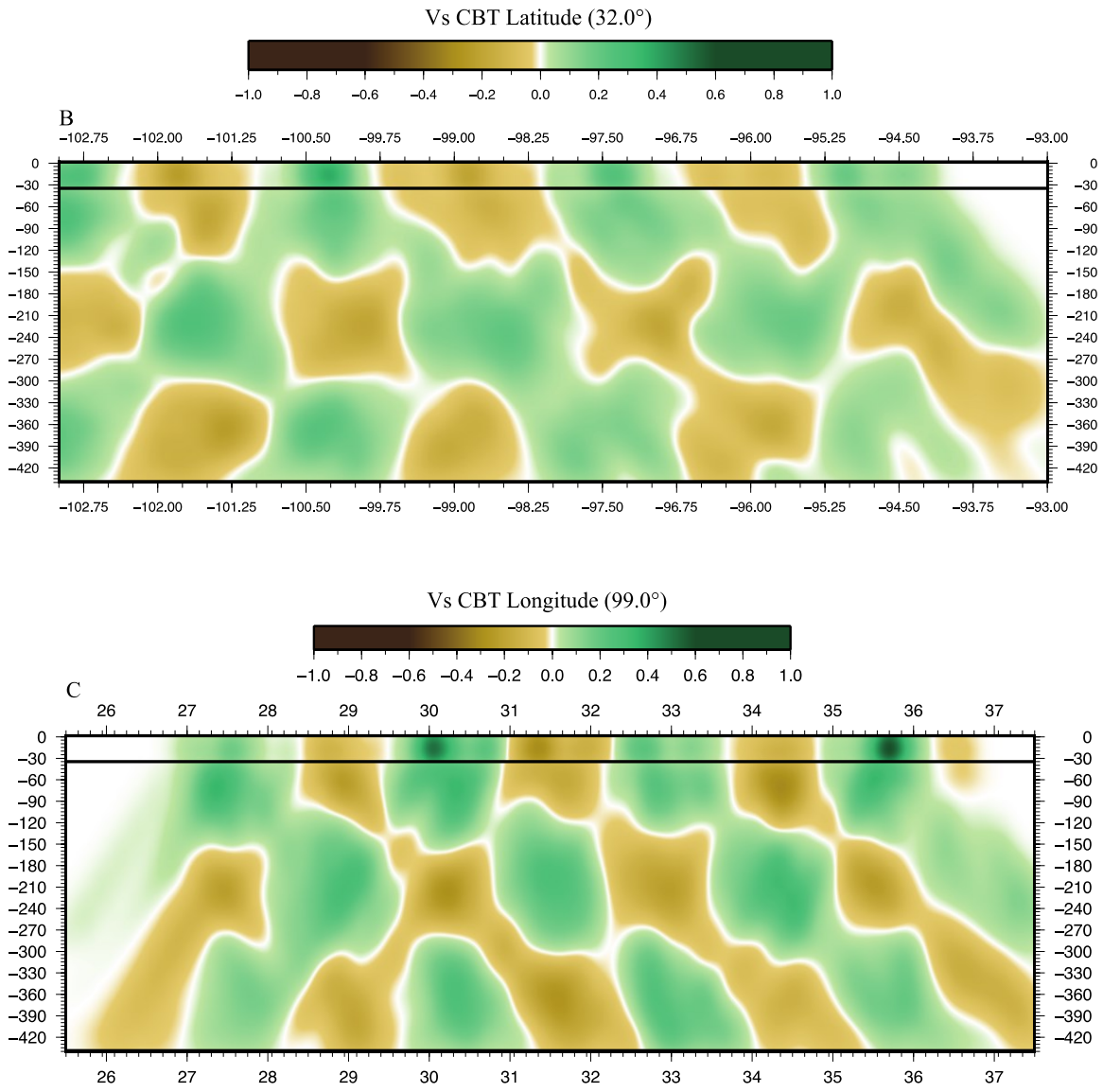

Figure 7: Vs checkerboard test result: (A) 75 km depth slice: displaying good resolution in the west of the study area with northeast-southwest smearing in the east, (B) Latitude (32.0°) slice displaying good resolution in the west of the study area and reasonable resolution in the east accompanied by little smearing, (C) Longitude (99.0°) slice displaying reasonable south to north resolution with some smearing (north to south).

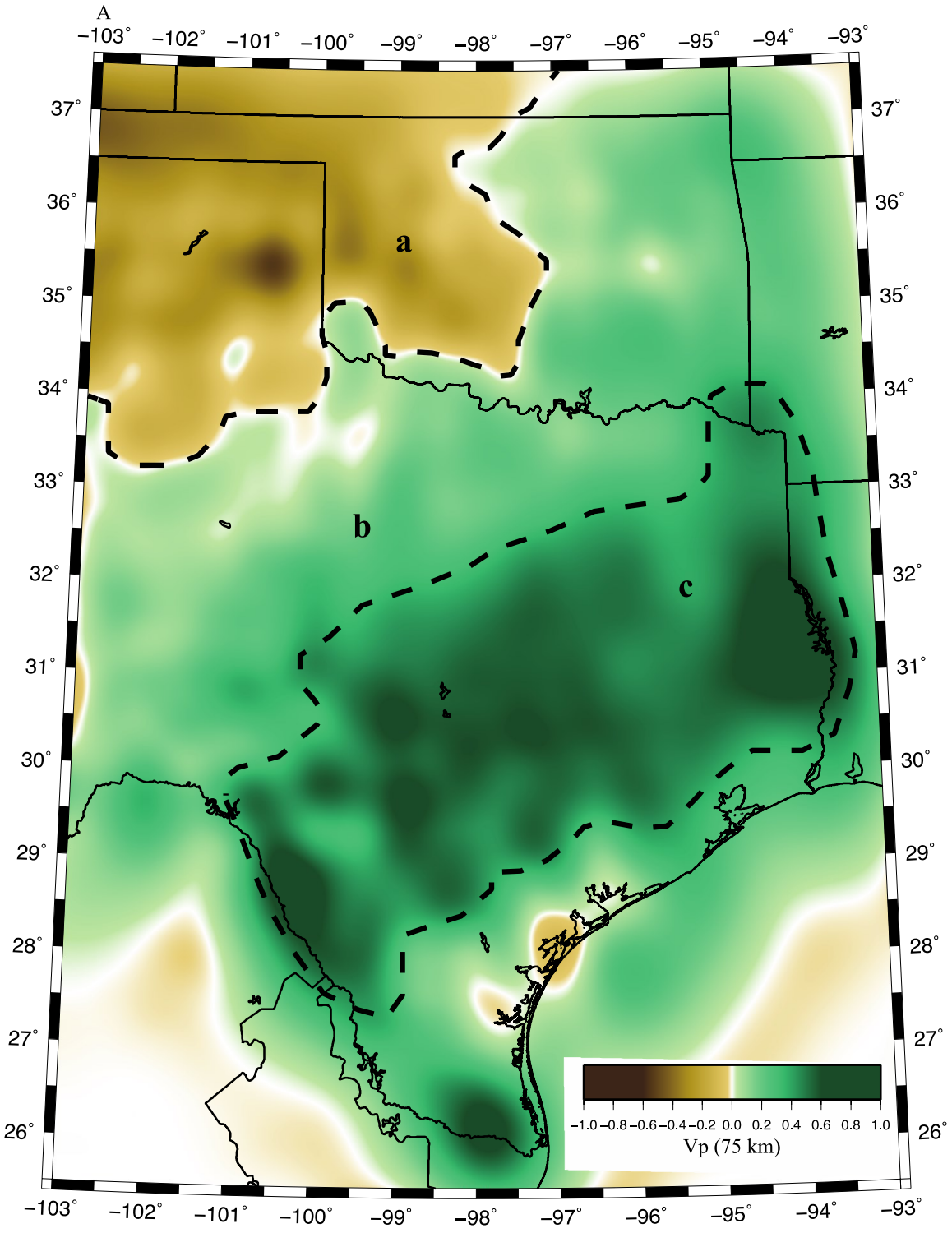
A
−103°
−102°
−101°
−100°
−99°
−98°
−97°
−96°
−95°
−94°
−93°
37°
36°
35°
34°
33°
32°
31°
30°
29°
28°
27°
26°
a
b
c
−1.0 −0.8 −0.6 −0.4 −0.2 0.0 0.2 0.4 0.6 0.8 1.0
Vp (75 km)

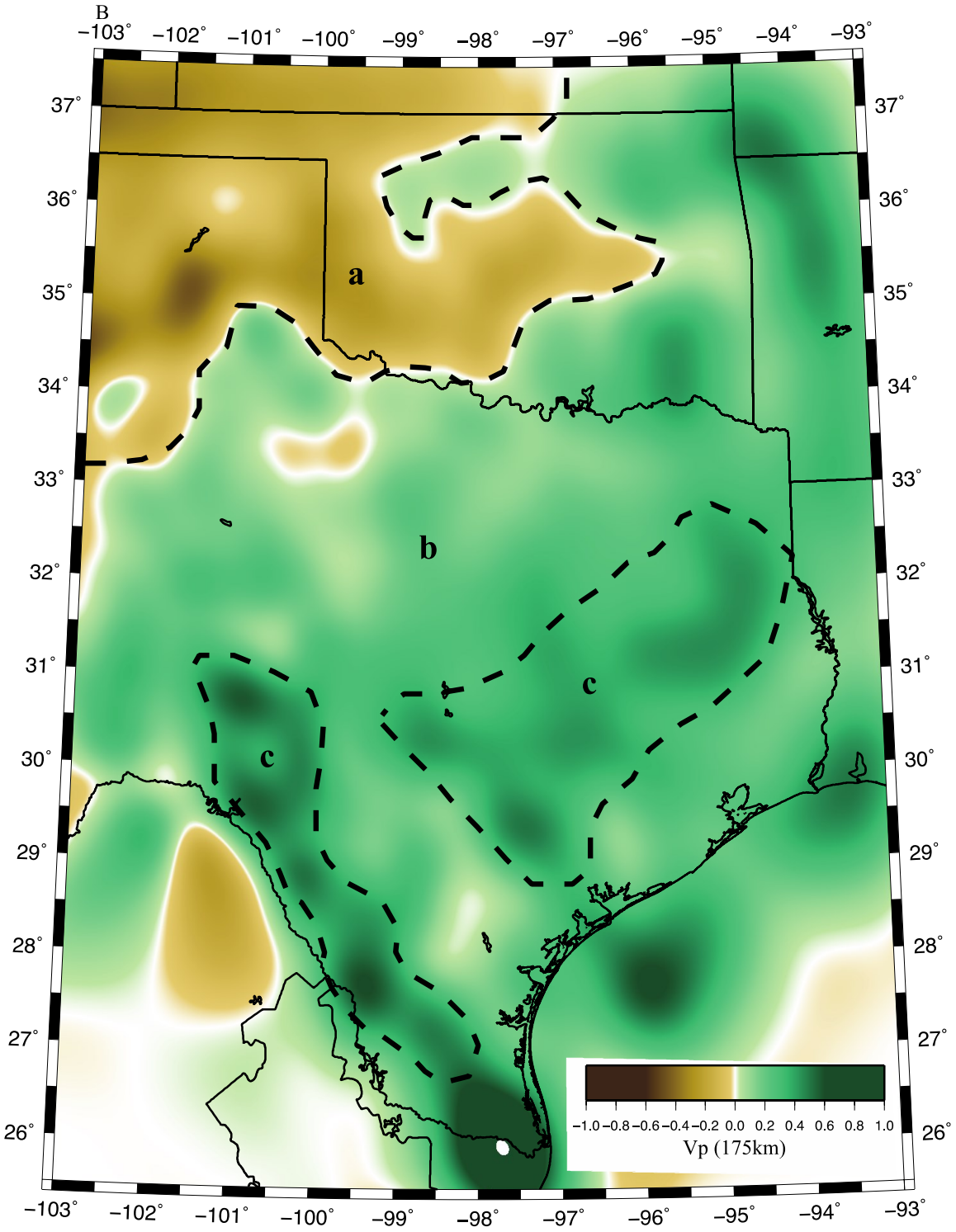
B
−103°
−102°
−101°
−100°
−99°
−98°
−97°
−96°
−95°
−94°
−93°
37°
36°
35°
34°
33°
32°
31°
30°
29°
28°
27°
26°
a
b
c
c
−1.0 −0.8 −0.6 −0.4 −0.2 0.0 0.2 0.4 0.6 0.8 1.0
Vp (175km)

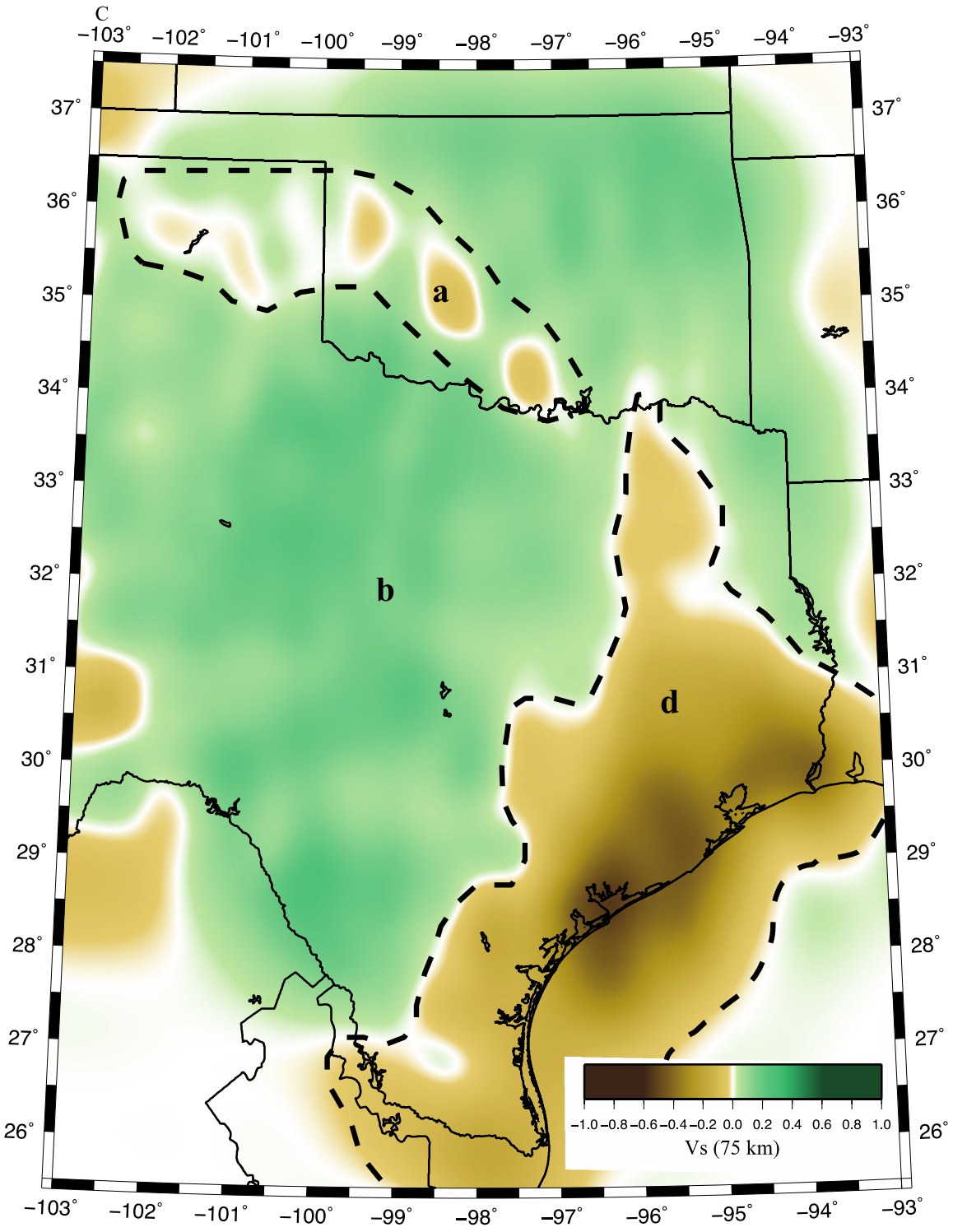
C
−103°
−102°
−101°
−100°
−99°
−98°
−97°
−96°
−95°
−94°
−93°
37°
36°
35°
34°
33°
32°
31°
30°
29°
28°
27°
26°
a
b
d
−1.0 −0.8 −0.6 −0.4 −0.2 0.0 0.2 0.4 0.6 0.8 1.0
Vs (75 km)

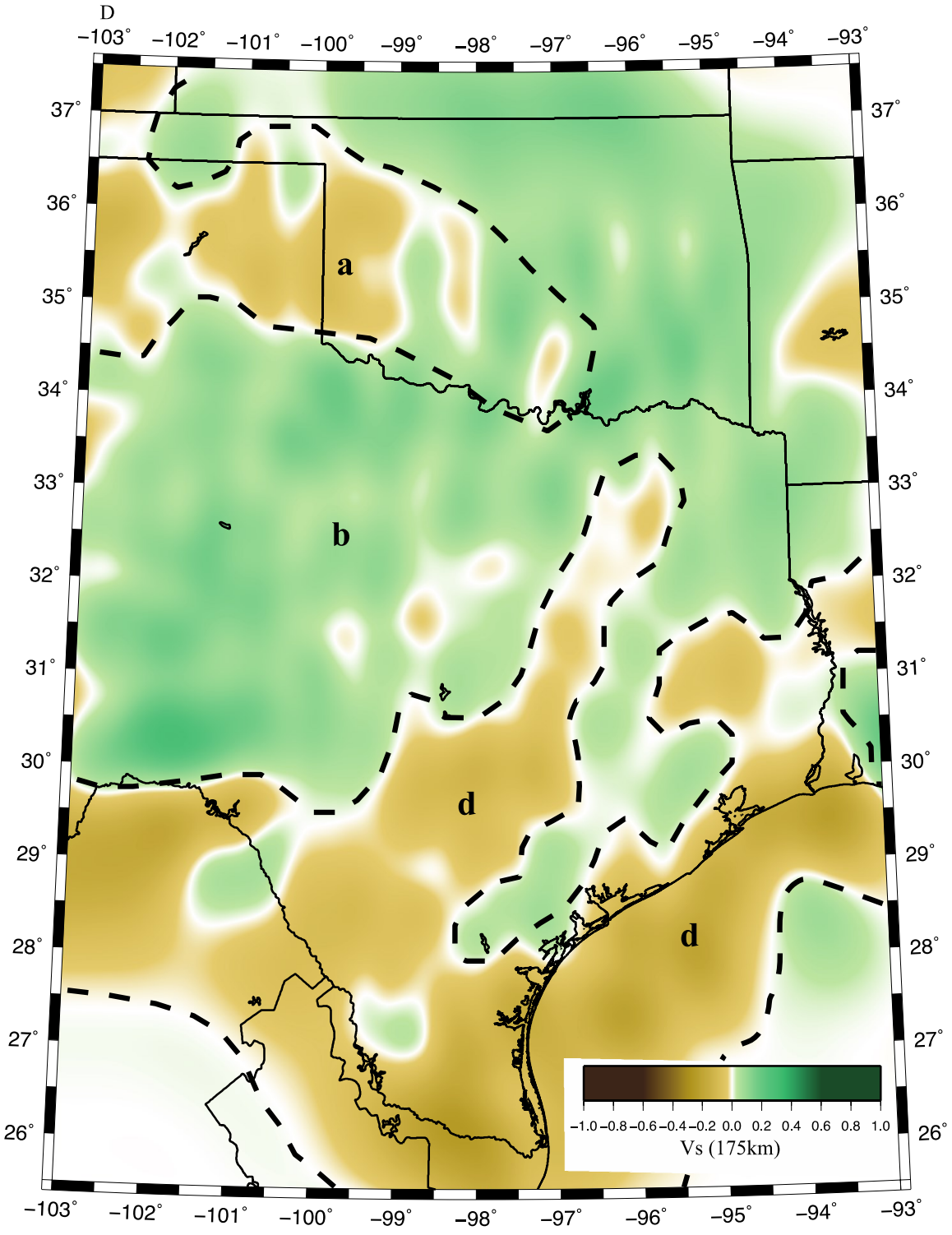

Figure 8: Depth slices of 3D tomography: (A) Vp depth slice (75 km) and (B) Vp depth slice (175 km): significant features are large slow anomaly, region a, present in the region of the Southern Oklahoma Aulacogen, large fast anomaly consistent with the southern extent of the Laurentia craton lithosphere, region b, and a high velocity anomaly, region c, in southeast Texas trending southwest-northeast. (C) Vs depth slice

(75 km) and (D) Vs depth slice (175 km): significant features are the slow anomalies, region a, which out line the Southern Oklahoma Aulacogen, the large fast anomaly, region b, consistent with the southern extent of the Laurentia craton, and a large slow anomaly, region d, which mimics the coastline and extending beneath the Laurentia craton.

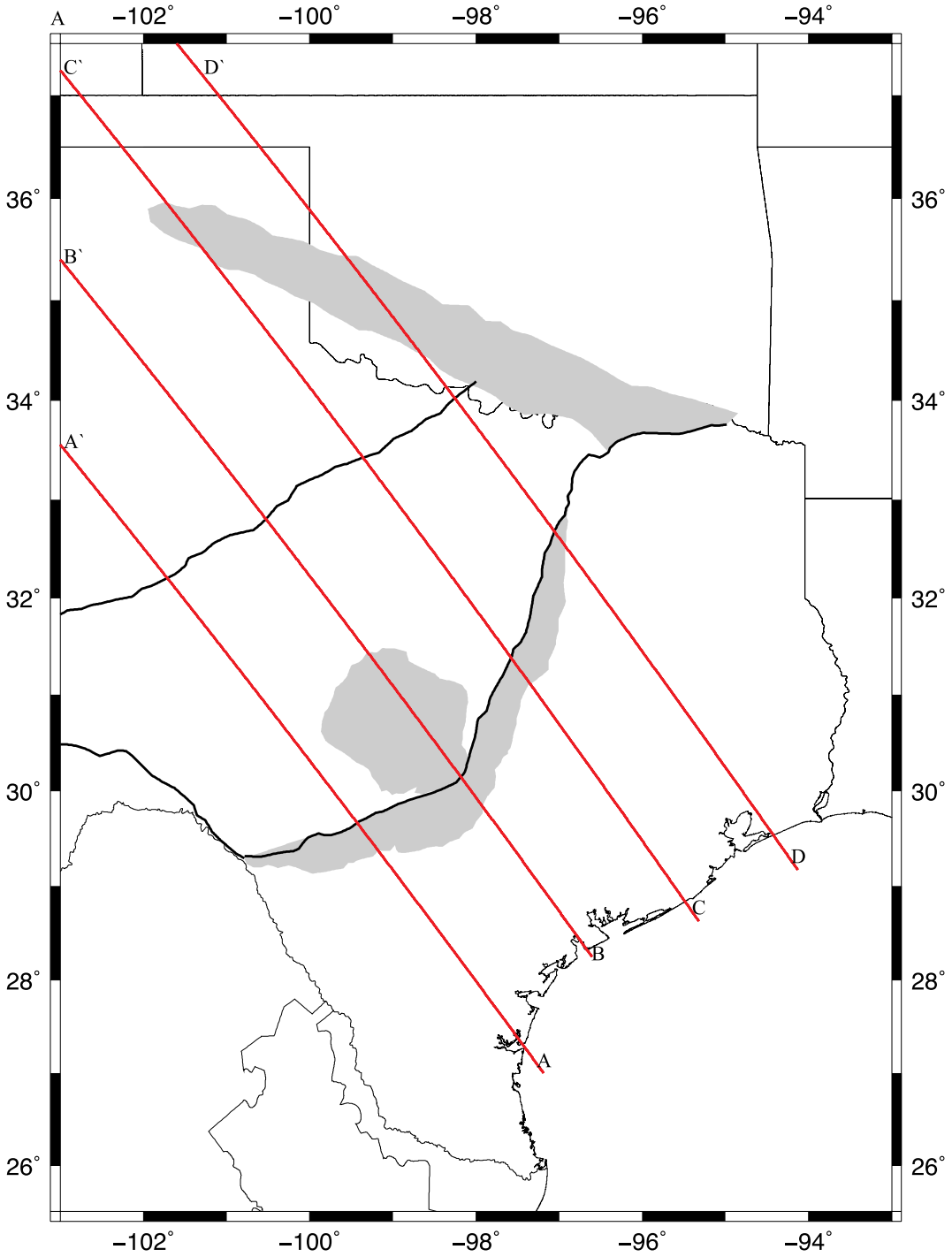

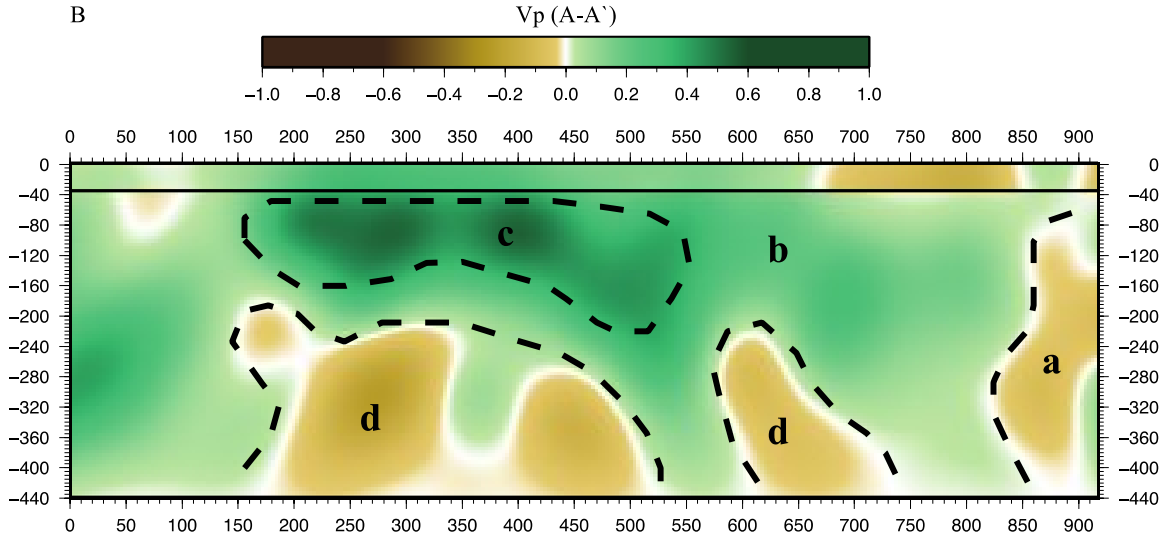
B
Vp (A-A`)
−1.0 −0.8 −0.6 −0.4 −0.2 0.0 0.2 0.4 0.6 0.8 1.0
0 50 100 150 200 250 300 350 400 450 500 550 600 650 700 750 800 850 900
0 −40 −80 −120 −160 −200 −240 −280 −320 −360 −400 −440
c
b
a
d
d

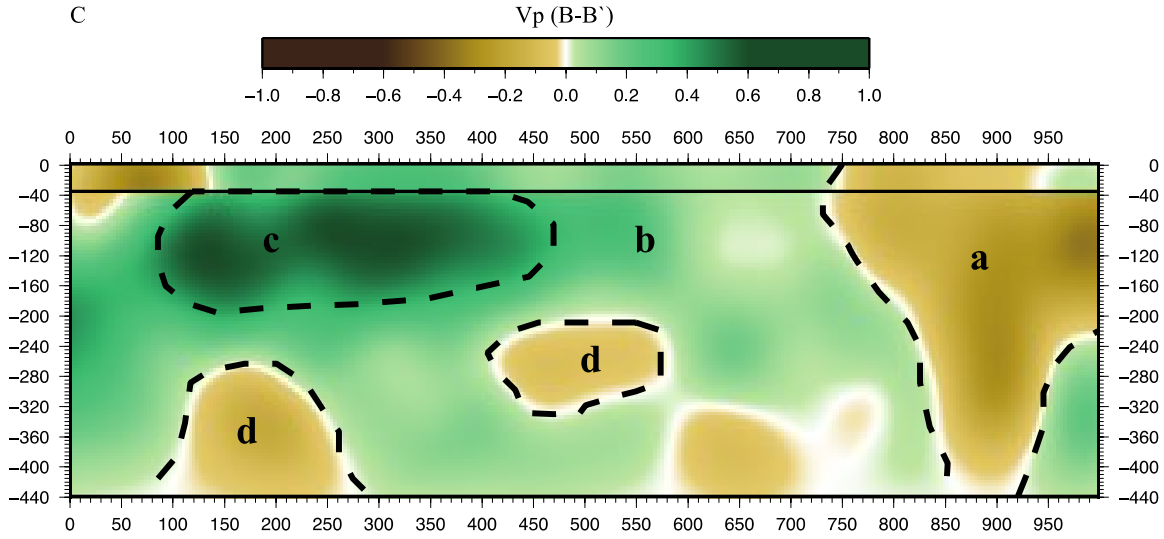
C
Vp (B-B`)
−1.0 −0.8 −0.6 −0.4 −0.2 0.0 0.2 0.4 0.6 0.8 1.0
0 50 100 150 200 250 300 350 400 450 500 550 600 650 700 750 800 850 900 950
0 −40 −80 −120 −160 −200 −240 −280 −320 −360 −400 −440
c
b
a
d
d

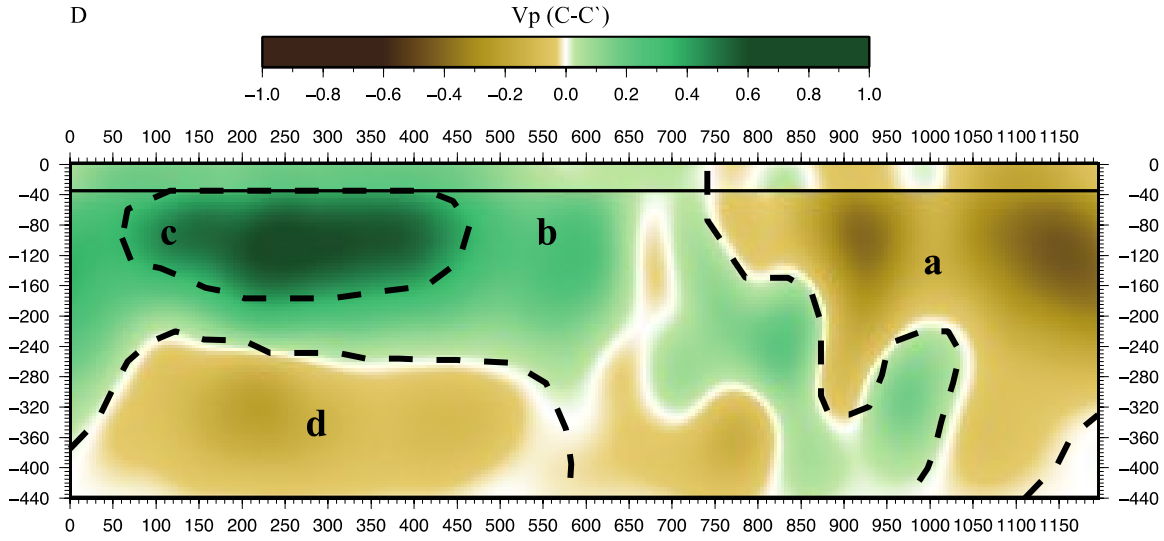
D
Vp (C-C`)
−1.0 −0.8 −0.6 −0.4 −0.2 0.0 0.2 0.4 0.6 0.8 1.0
0 50 100 150 200 250 300 350 400 450 500 550 600 650 700 750 800 850 900 950 1000 1050 1100 1150
0 −40 −80 −120 −160 −200 −240 −280 −320 −360 −400 −440
c
b
a
d

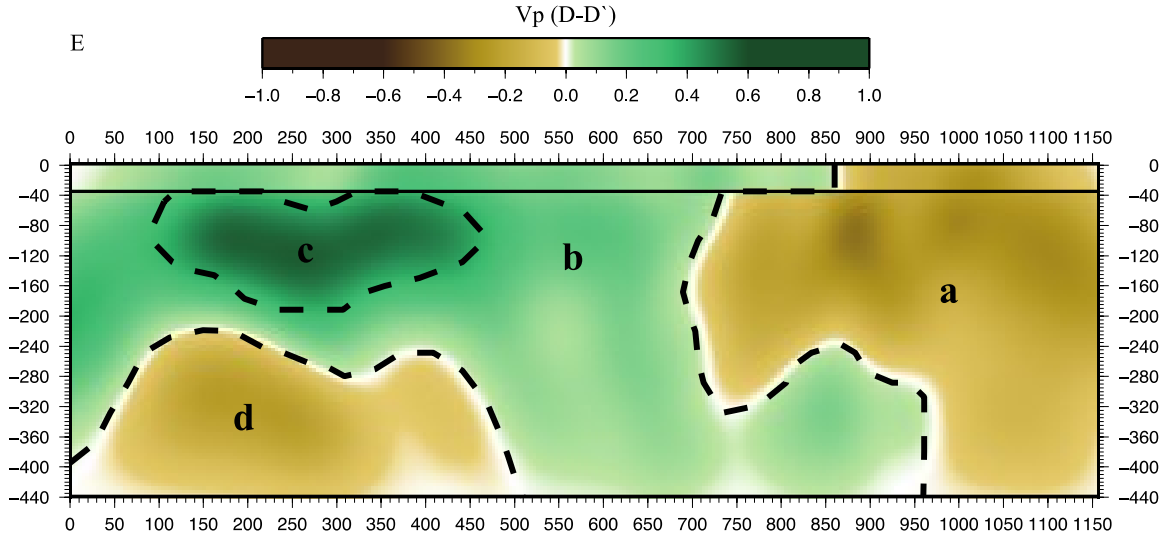
E
Vp (D-D`)
−1.0 −0.8 −0.6 −0.4 −0.2 0.0 0.2 0.4 0.6 0.8 1.0
0 50 100 150 200 250 300 350 400 450 500 550 600 650 700 750 800 850 900 950 1000 1050 1100 1150
0 −40 −80 −120 −160 −200 −240 −280 −320 −360 −400 −440
c
b
a
d

F

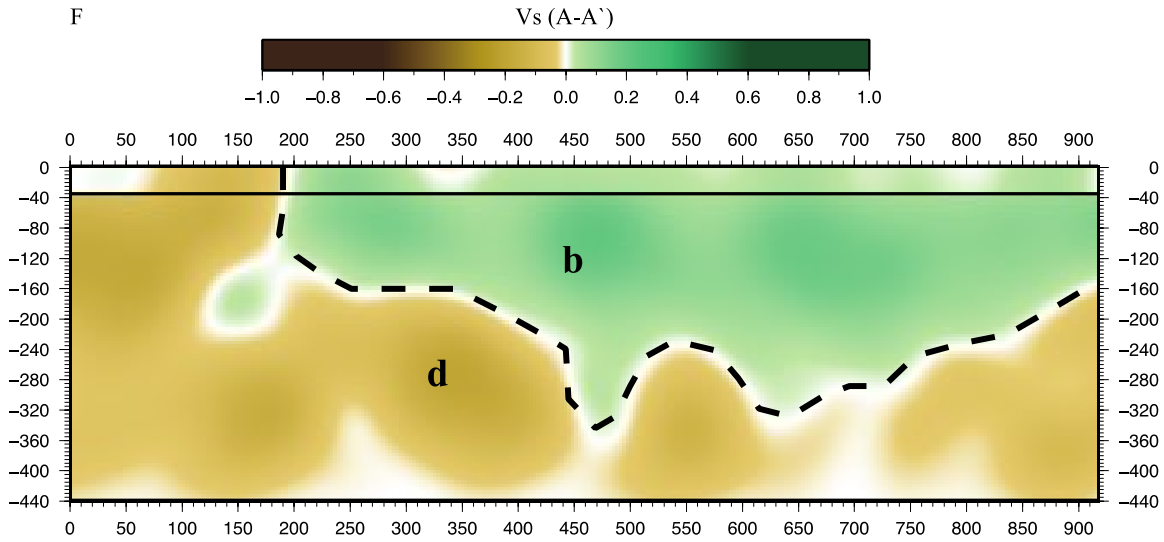
Vs (A-A`)
−1.0 −0.8 −0.6 −0.4 −0.2 0.0 0.2 0.4 0.6 0.8 1.0
0 50 100 150 200 250 300 350 400 450 500 550 600 650 700 750 800 850 900
0 −40 −80 −120 −160 −200 −240 −280 −320 −360 −400 −440
b
d

G

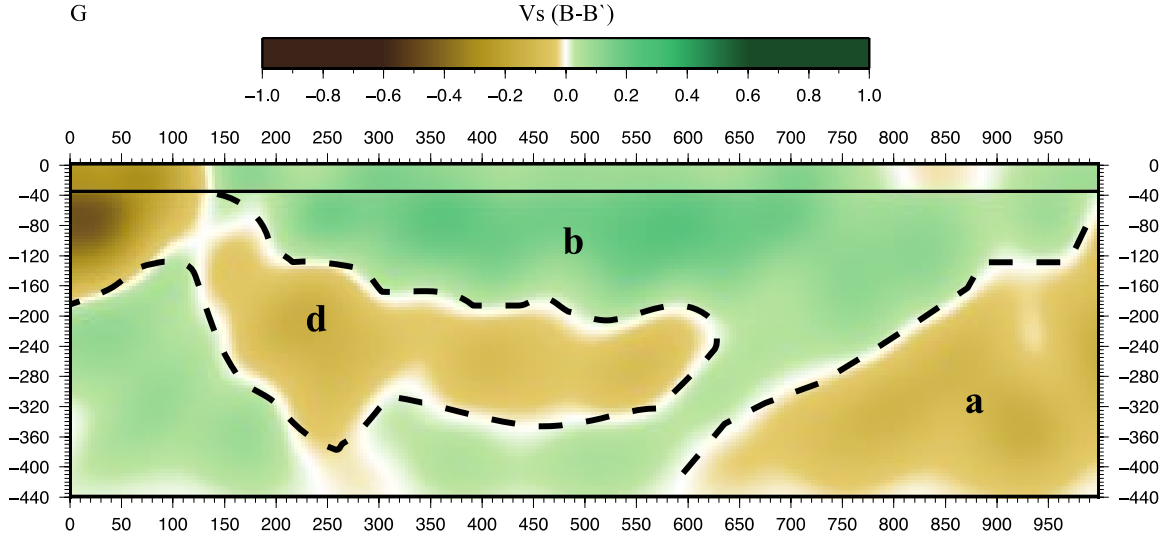
Vs (B-B`)
−1.0 −0.8 −0.6 −0.4 −0.2 0.0 0.2 0.4 0.6 0.8 1.0
0 50 100 150 200 250 300 350 400 450 500 550 600 650 700 750 800 850 900 950
0 −40 −80 −120 −160 −200 −240 −280 −320 −360 −400 −440
b
d
a

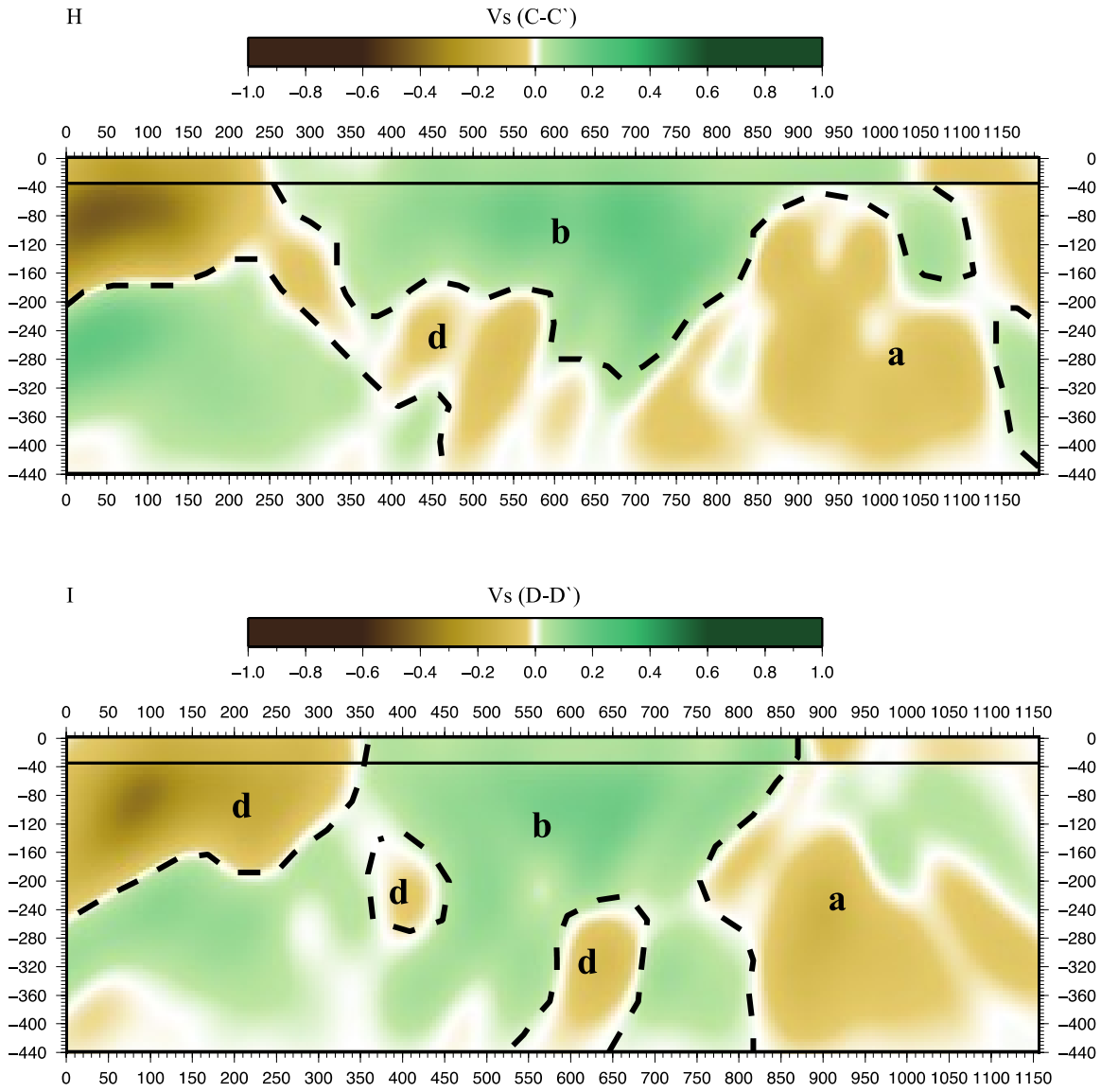

Figure 9: 2D Great-Circle cross-sections: (A) Map view of A-A`, B-B`, C-C` and D-D` cross-section locations with significant tectonic features. (B) A-A`, (C) B-B', (D) C-C` and (E) D-D`: great-circles through Vp model displaying a fast anomaly, region b, associated with the southern extent of the Laurentia craton, large slow anomaly, region d, at the bottom of the model associated with the a LAB shear zone, and a low velocity vertical anomaly, region a, in the region of the Southern Oklahoma Aulacogen. (F) A-A`, (G) B-B`, (H) C-C` and (I) D-D`: great-circles through Vs model displaying a fast anomaly, region b, associated with the southern extent of the Laurentia craton, a slow velocity anomaly, region d, consistent with the LAB shear zone and the Gulf Coast sediments, and a slow velocity vertical anomaly in the region of the Southern Oklahoma Aulacogen.

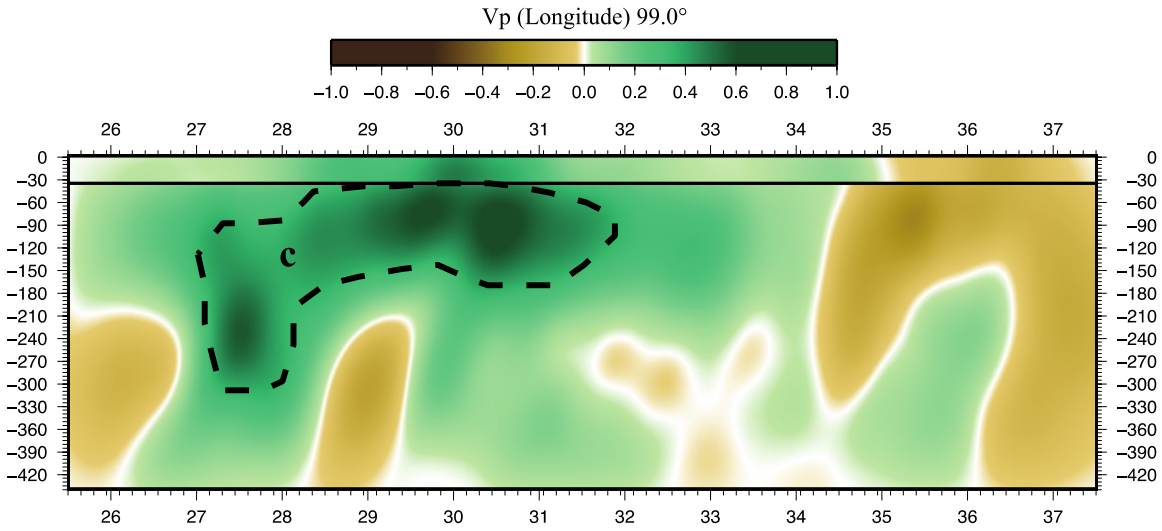

Figure 10: 2D Longitude (99.0°) slice: Cross-section through 3D Vp tomography, fast anomaly (dark green) extending down and the slow velocity material (tan) is ascending to fill the void.

CHAPTER THREE

Conclusions

The research presented in this study, allows the scientific community to have a more clear understanding of the deep subsurface structures beneath Texas and Oklahoma. This, ongoing, and future geophysical research done, will undoubtedly shed new light on scientific problems we, as the scientific community, have yet to solve, while simultaneously proposing new and interesting questions, for the future researches at Baylor University to answer.